Water Mass Transformations Within Antarctic Coastal Polynyas of Prydz Bay from Clustered Drifters

Margaret Murakami[1], Aleksi Nummelin[2], Benjamin Keith Galton-Fenzi[3], and Petteri Uotila[4]

[1]University of Texas at Austin
[2]University of Oslo
[3]Australian Antarctic Division
[4]University of Helsinki

September 7, 2023

Abstract

Antarctic Bottom Water (AABW) forms the deepest limb of the meridional overturning circulation (MOC) and is a key control on global exchanges of heat, freshwater, and carbon. Density differences that drive the MOC have their origin, in part, in coastal polynyas. Prydz Bay polynyas in East Antarctica are a key source of Dense Shelf Water (DSW) that feeds AABW to the Atlantic and Indian Oceans. However, several poorly understood mechanisms influence the pathways and change water mass properties of the DSW on its way to the abyss. To better understand these mechanisms, we release Lagrangian particles in a 10 km resolution simulation of the Whole Antarctic Ocean Model and analyze the resulting tracks using novel cluster analysis. Our results highlight the role of mixing with other water masses on the shelf in controlling the fate of DSW and its eventual contribution to AABW. When advected beneath the ice shelf, DSW can mix with fresh Ice Shelf Water (ISW), becoming less dense and making future AABW formation less likely. This study confirms that towards the shelf break along the Antarctic Slope Current, mixing with circumpolar deep water (CDW) forms modified circumpolar deep water (mCDW) and influences DSW export as AABW. Our findings indicate that the pathway from DSW to AABW is sensitive to mixing with ambient waters on the shelf. An important implication is that with future increase in ice shelf melt and CDW warming, AABW production is likely to decline, even if DSW production in coastal polynyas remains constant.

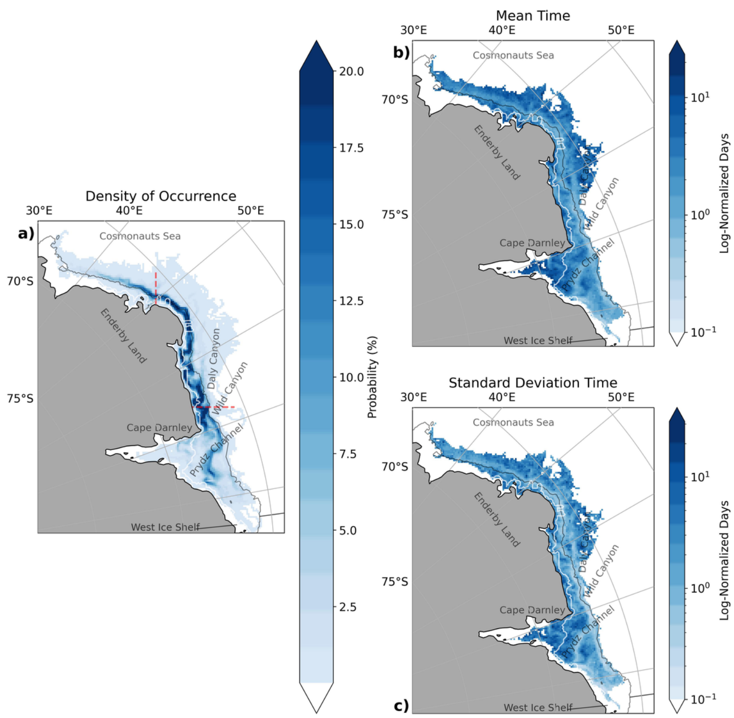
Density of Occurrence
a)
Cosmonauts Sea
Enderby Land
Daly Canyon
Wild Canyon
Cape Darnley
Prydz Channel
West Ice Shelf
30°E
40°E
50°E
70°S
75°S
Probability (%)
20.0
17.5
15.0
12.5
10.0
7.5
5.0
2.5
Mean Time
b)
Standard Deviation Time
c)
Log-Normalized Days
10^1
10^0
10^{-1}

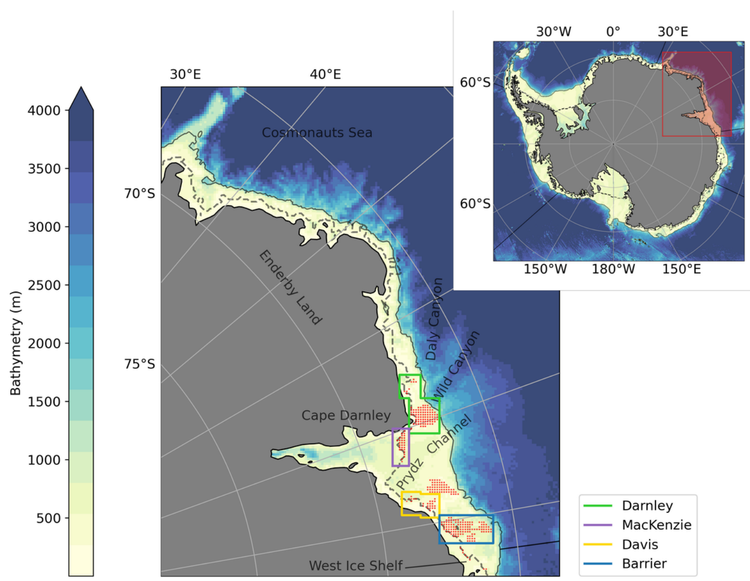
Bathymetry (m)
4000
3500
3000
2500
2000
1500
1000
500
30°E
40°E
70°S
75°S
Cosmonauts Sea
Enderby Land
Daly Canyon
Wild Canyon
Cape Darnley
Prydz Channel
West Ice Shelf
Darnley
MacKenzie
Davis
Barrier
30°W
0°
30°E
60°S
150°W
180°W
150°E

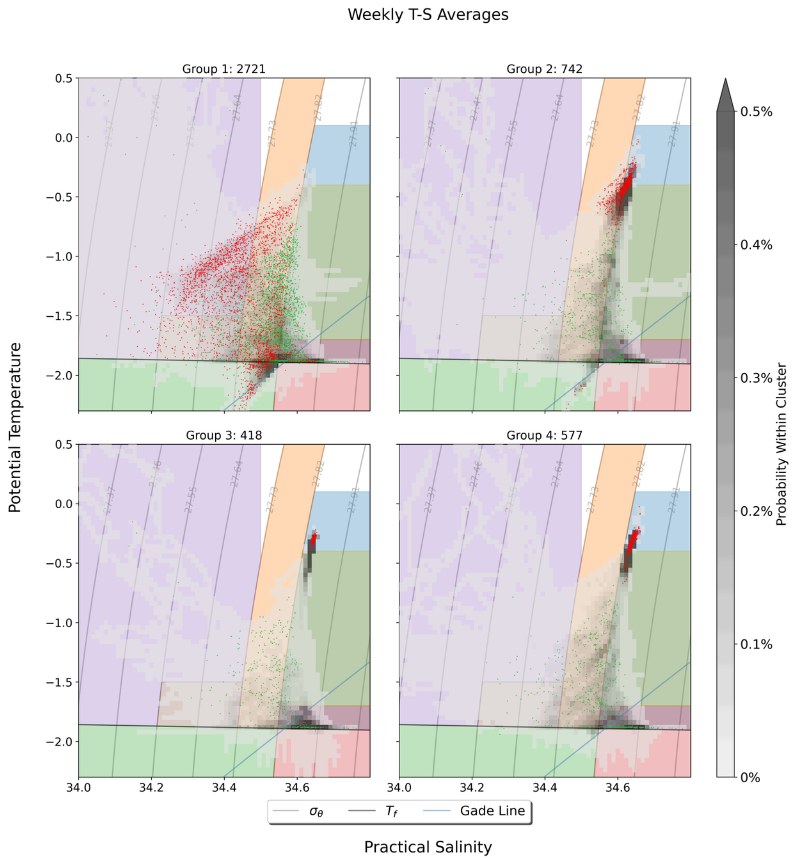
Weekly T-S Averages
Group 1: 2721
Group 2: 742
Group 3: 418
Group 4: 577
Potential Temperature
Practical Salinity
Probability Within Cluster
0.5%
0.4%
0.3%
0.2%
0.1%
0%
σ_θ
T_f
Gade Line

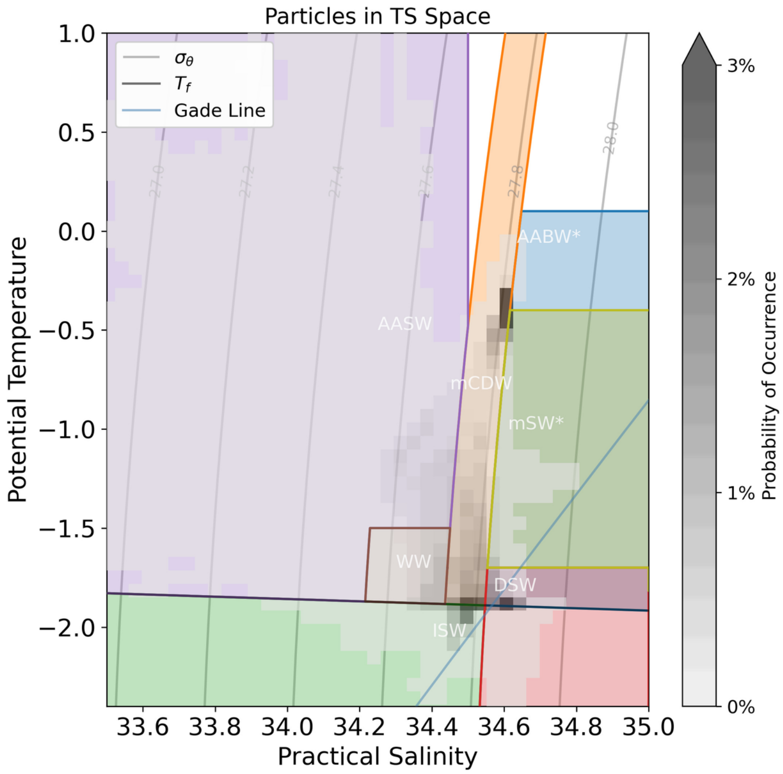

Particles in TS Space
Potential Temperature
Practical Salinity
Probability of Occurrence
AASW
mCDW
mSW*
AABW*
WW
DSW
ISW
Gade Line

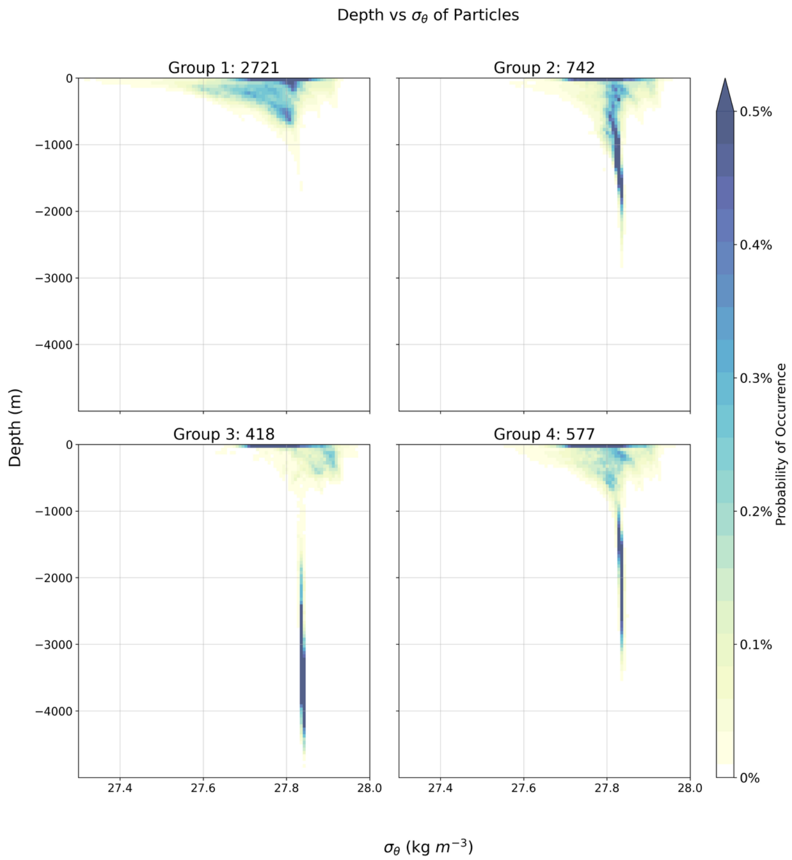

Depth vs σ_θ of Particles
Group 1: 2721
Group 2: 742
Group 3: 418
Group 4: 577
Depth (m)
0
−1000
−2000
−3000
−4000
27.4
27.6
27.8
28.0
σ_θ (kg m^{-3})
Probability of Occurrence
0.5%
0.4%
0.3%
0.2%
0.1%
0%

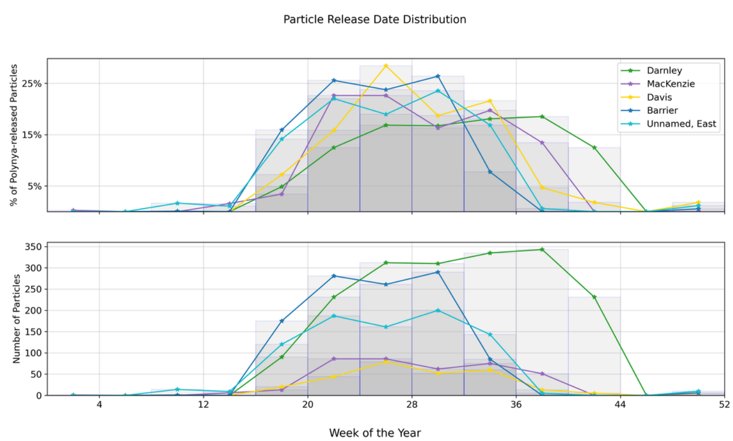

Particle Release Date Distribution
Darnley
MacKenzie
Davis
Barrier
Unnamed, East
% of Polynya-released Particles
25%
15%
5%
Number of Particles
350
300
250
200
150
100
50
0
4
12
20
28
36
44
52
Week of the Year

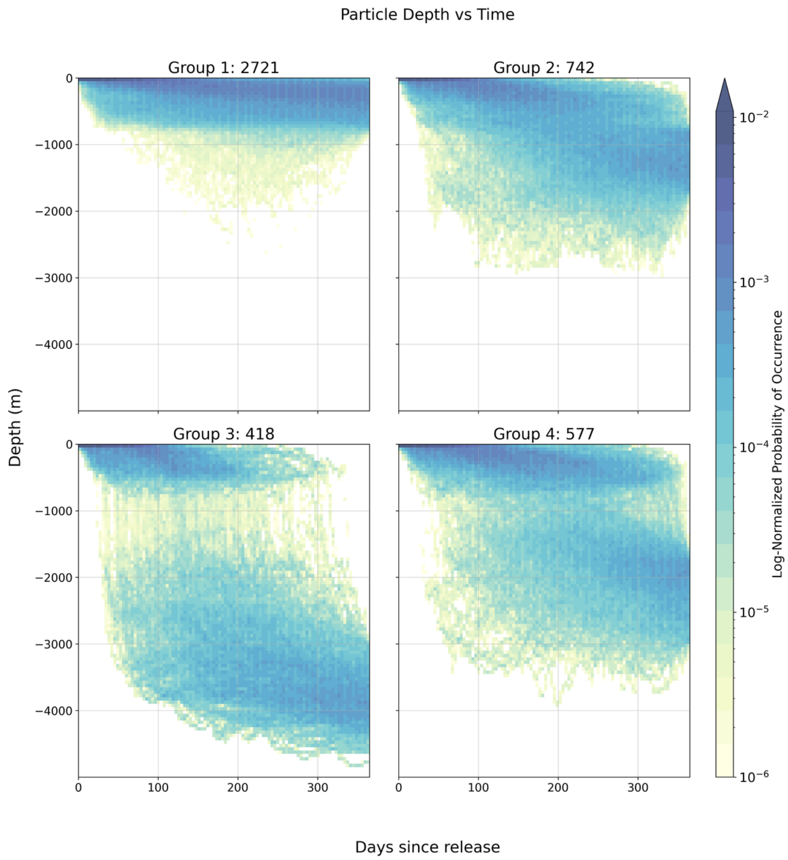
Particle Depth vs Time
Group 1: 2721
Group 2: 742
Group 3: 418
Group 4: 577
Depth (m)
0
−1000
−2000
−3000
−4000
0
100
200
300
Days since release
Log-Normalized Probability of Occurrence
10^{-2}
10^{-3}
10^{-4}
10^{-5}
10^{-6}

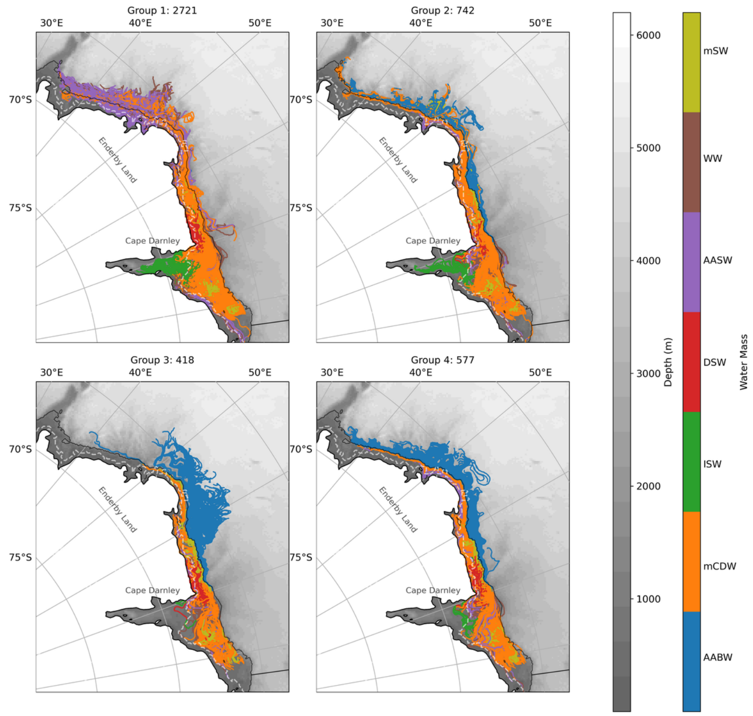
Group 1: 2721
Group 2: 742
Group 3: 418
Group 4: 577
30°E
40°E
50°E
70°S
75°S
Enderby Land
Cape Darnley
Depth (m)
Water Mass
mSW
WW
AASW
DSW
ISW
mCDW
AABW

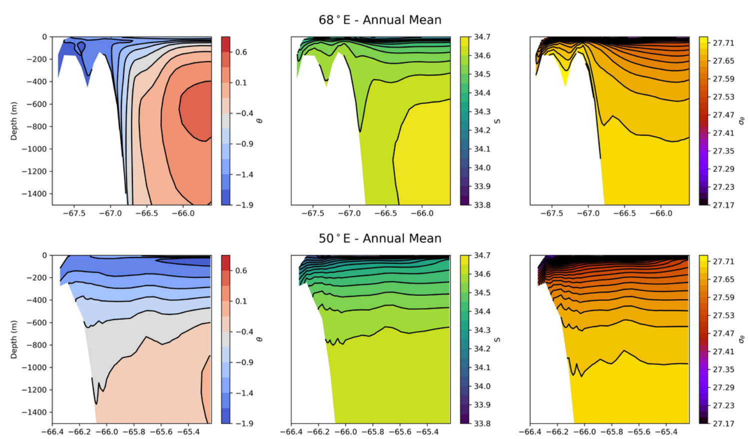
68 ° E - Annual Mean
50 ° E - Annual Mean
Depth (m)
Latitude

Water Mass Transformations Within Antarctic Coastal Polynyas of Prydz Bay from Clustered Drifters

Margaret Murakami[1,2], Aleksi Nummelin[3,4], Benjamin Keith Galton-Fenzi[5,6,7], Petteri Uotila[1]

[1]Physics, Institute for Atmospheric and Earth System Research, University of Helsinki, Helsinki, Finland
[2]Jackson School of Geosciences, The University of Texas at Austin, Austin, TX, USA
[3]Finnish Meteorological Institute, Helsinki, Finland
[4]Norwegian Research Centre AS and Bjerknes Centre for Climate Research, Bergen, Norway
[5]Australian Antarctic Division, Kingston, TAS, Australia
[6]Australian Antarctic Program Partnership, Institute for Marine and Antarctic Studies, University of Tasmania, nipaluna/Hobart, TAS, Australia
[7]Australian Centre for Excellence in Antarctic Science, University of Tasmania, nipaluna/Hobart, TAS, Australia

Key Points:

- Lagrangian particles show how Dense Shelf Water from Prydz Bay transforms along its way from the continental shelf to the abyssal ocean.
- Interactions between Amery Ice Shelf meltwater and upwelled circumpolar deep water influence the formation and export of Dense Shelf Water.
- Along isopycnal rather than diapycnal mixing is primarily responsible for transforming Dense Shelf Water into Antarctic Bottom Water.

Corresponding author: Margaret Murakami, mmurakami@utexas.edu

Abstract

Antarctic Bottom Water (AABW) forms the deepest limb of the meridional overturning circulation (MOC) and is a key control on global exchanges of heat, freshwater, and carbon. Density differences that drive the MOC have their origin, in part, in coastal polynyas. Prydz Bay polynyas in East Antarctica are a key source of Dense Shelf Water (DSW) that feeds AABW to the Atlantic and Indian Oceans. However, several poorly understood mechanisms influence the pathways and change water mass properties of the DSW on its way to the abyss. To better understand these mechanisms, we release Lagrangian particles in a 10 km resolution simulation of the Whole Antarctic Ocean Model and analyze the resulting tracks using novel cluster analysis. Our results highlight the role of mixing with other water masses on the shelf in controlling the fate of DSW and its eventual contribution to AABW. When advected beneath the ice shelf, DSW can mix with fresh Ice Shelf Water (ISW), becoming less dense and making future AABW formation less likely. This study confirms that towards the shelf break along the Antarctic Slope Current, mixing with circumpolar deep water (CDW) forms modified circumpolar deep water (mCDW) and influences DSW export as AABW. Our findings indicate that the pathway from DSW to AABW is sensitive to mixing with ambient waters on the shelf. An important implication is that with future increase in ice shelf melt and CDW warming, AABW production is likely to decline, even if DSW production in coastal polynyas remains constant.

Plain Language Summary

Antarctic Bottom Water (AABW) helps drive the meridional overturning circulation (MOC), regulating global exchanges of ocean properties and Southern Ocean exchanges of heat and salt between distinct bodies of water or water masses. Coastal polynyas—regions of ice-free open ocean—feature continuous sea ice formation in winter and expel salt into the water column. Some water formed in these polynyas is dense enough to sink to the abyssal ocean, forming AABW, but the factors which affect this process are not well understood. Here, we investigate the influences of regional differences and mixing with other water masses on the trajectories of water originating from coastal polynyas in Prydz Bay, East Antarctica by tracking virtual water particles in a regional ocean model. Mixing between dense water from Prydz Bay with either ice shelf meltwater or warm water upwelled during the MOC can control the export of dense water to the deep ocean; if ice shelf melt intensifies according to climate predictions, this factor could limit future AABW formation. Water particles from Prydz Bay typically follow the Antarctic continental shelf before moving either along the ocean surface or through subsea canyons to the abyss.

1 Introduction

Antarctic bottom water (AABW) is the densest water mass in the global ocean and is created as it sinks from the continental slope to the deep ocean (Orsi et al., 1999). Recent studies have underlined changes to AABW temperature, salinity, and volume (Purkey & Johnson, 2013; Schmidtko et al., 2014; van Wijk & Rintoul, 2014; Anilkumar et al., 2021; Zhou et al., 2023). The declining formation rate of AABW in response to these changes has implications for the global sea level (Purkey & Johnson, 2013), the Southern Annular Mode (Schroeter et al., 2022), and the Meridional Overturning Circulation (MOC) (Gunn et al., 2023). Circulation on the Antarctic shelf, and particularly the interactions between offshore and onshore shelf waters (Gill, 1973; Orsi et al., 1999; Silvano et al., 2018) and glacial meltwater (Abernathey et al., 2016; Pellichero et al., 2018; Li et al., 2023) have been linked to modification of exported deep water and changes to Southern Ocean overturning. While recent developments in understanding abyssal overturning have been made, in situ observations remain sparse and with a summer bias (Heywood et al., 2014). Consequently, our understanding of the connections between the processes at the Antarctic margin with the abyssal ocean is insufficient to help constrain and predict the behavior of the ice sheet and response of the global oceans.

Abyssal export of AABW begins at the Antarctic margin, where Water Mass Transformations (WMTs) occur to alter the physical qualities of on-shelf water. The dominant origin of AABW lies within coastal polynyas: ice-free open water which exposes the ocean surface to negative atmospheric heat fluxes and features continuous sea ice formation and brine rejection in winter (Tamura et al., 2008, 2011). The ocean buoyancy loss in these regions drives the production of High Salinity Shelf Water (HSSW) and later Dense Shelf Water (DSW) (Martin, 2019; Solodoch et al., 2022), which can be transported westward by the Antarctic Slope Current (ASC) along the continental shelf (Nunes Vaz & Lennon, 1996; Peña-Molino et al., 2016) or into the sub-ice cavity (Herraiz-Borreguero et al., 2015). DSW can either mix with Circumpolar Deep Water (CDW) upwelled on steeply-tilted isopycnals (Liu et al., 2017; Thompson et al., 2018; Guo et al., 2019) or cascade down the continental shelf forming AABW (Baines & Condie, 1985; Shanmugam, 2021). Thus, AABW formation connects surface processes in the Southern Ocean to the circulation of the deep ocean (Orsi et al., 1999; Jacobs, 2004) and regulates the ventilation of abyssal waters (Sallée et al., 2010).

The extent to which the Southern Ocean impacts the Earth's climate system—including controlling the Meridional Overturning Circulation (MOC) and absorbing heat from the atmosphere—thus depends in part on the formation of DSW along the Antarctic coast in coastal polynyas and its ultimate conversion to AABW. Tamura et al. (2016) suggests that decreases in sea ice extent increase the total sea ice production (SIP) of some latent heat polynyas, in turn altering the formation of DSW. Given that polynyas alter the salt and heat flux to coastal waters (Tamura et al., 2008, 2011), polynyas can alter the circulation of the Southern Ocean. The evolution of DSW from polynyas is complex, and understanding the mechanisms which control and contribute to AABW formation is important for predicting changes in global overturning circulation as well as for tracking the ocean heat and carbon uptake. Several hypotheses exist surrounding these WMTs: recent studies have shown that Ice Shelf Water (ISW) and shelf-modified Circumpolar Deep Water (mCDW) can influence the formation of sea ice (Guo et al., 2019) as well as DSW (Herraiz-Borreguero et al., 2016; Narayanan et al., 2019). Bottom topography also impacts the export of AABW to ocean depths (Baines & Condie, 1985; Amblas & Dowdeswell, 2018), and Portela et al. (2022) confirms that the transformation of DSW to AABW is spatially dependent and influenced by changes in bathymetry.

The Eastern Antarctic Prydz Bay (Figure 1) is a notable exporter of DSW, with several highly productive major and minor polynyas that contribute AABW to both the Atlantic and Indian Oceans (Ohshima et al., 2016; Solodoch et al., 2022). One such polynya at the Western edge of Prydz Bay, the Cape Darnley polynya, accounts for up to 13% of all AABW produced around Antarctica (Ohshima et al., 2013). Similarly, Tamura et al. (2008) showed that the MacKenzie polynya is one of the greatest producers of sea ice throughout the Southern Ocean. The high productivity of these areas for DSW formation is very likely enhanced by the export of cold shelf waters flowing from the Amery Depression and not just from the polynya activity (Foldvik et al., 2004; Lacarra et al., 2014; Dinniman et al., 2020). Other named polynyas include the Davis and Barrier polynyas to the East of the Prydz channel, both highly productive sites for sea ice (Kusahara et al., 2010). Combined with other unnamed seasonal polynyas, each of these is capable of contributing to DSW production and downslope flows of AABW (Jia et al., 2022). Several studies suggest a net westward transport along the continental shelf and slope in the East Antarctic region (Thompson et al., 2018; Dawson et al., 2023), but a better understanding of the export trajectories for DSW from the Prydz Bay polynya region is still needed to provide insight into the factors which inhibit or promote the formation of AABW.

High-resolution ocean model outputs using Lagrangian particles are a powerful tool to help identify the complex processes of WMT in the Southern Ocean where data are otherwise limited. Previous works utilizing Lagrangian approaches have studied Southern Ocean upwelling and associated WMT (Viglione & Thompson, 2016; Tamsitt et al., 2018). The work by van Sebille et al. (2013) also utilized Lagrangian tracking to study the formation of AABW around the continent. Studies have also considered the transport of AABW using both computational models (Solodoch et al., 2022; Li et al., 2023) and observational data (Gunn et al., 2023). While additional tracers have been used to investigate shelf circulation by Dinniman et al. (2020), abyssal overturning has not yet been studied using Lagrangian tools, leaving a gap in the current understanding of the connection between the Antarctic shelf current and the abyssal circulation. As van Sebille et al. (2018) note, ocean circulation can operate within a large range of scales, and using an ensemble of Lagrangian particles can help to represent the diversity of fluid motion. Furthermore, inferring Southern Ocean currents using simulated Lagrangian particles can determine the relative interconnectivity of ocean basins (Dawson et al., 2023), isopycnal mixing (Abernathey et al., 2022), and represent the vertical and horizontal mixing of water masses in greater detail (Viglione & Thompson, 2016).

This study utilizes Lagrangian analysis to explore the transport of polynya-sourced water in the Prydz Bay region and its transformation to AABW. The resulting three-dimensional trajectories of Lagrangian particles shed light on the processes which influence DSW export from the East Antarctic continental shelf as well as those which affect the eventual formation of AABW. Furthermore, by clustering the drifters and associated water mass properties, we investigate the bathymetric variability, shelf geography, and buoyancy forcing that influence the formation of AABW from polynya-sourced water. Synthesizing the connections between the formation of DSW from coastal polynyas with the downstream formation of AABW improves present understanding of the physical processes which regulate dense water transport around the Antarctic continent.

Our paper is organized as follows: section 2 describes the model configuration and Lagrangian setup, as well as the clustering algorithms used. section 3.1 presents mean pathways and WMTs of the entire model results while section 3.2 shows how clustered drifters elucidate key overturning processes. In section 4, the results are investigated in further detail and compared with results of other studies. A brief set of conclusions is provided in section 5.

2 Model and Methods

2.1 Model description, domain, and design

The Whole Antarctic Ocean Model (WAOM v1.0; Richter et al. (2022)) was developed from the Ice Shelf version of the Regional Ocean Modeling System (ROMS 3.6), a free-surface, primitive equations model which follows the terrain of the ocean floor (Galton-Fenzi et al., 2012; Dinniman et al., 2007; Shchepetkin & McWilliams, 2009). The algorithms in ROMS use a discretized version of the Reynolds-averaged Navier-Stokes equations that describe the evolution of temperature, salinity, and other variables, over time. ROMS uses a Boussinesq approximation that density is constant except when it appears in equations determined by gravitational force, and that mass conservation is interchangeable with volume conservation in the equations of state (Shchepetkin & McWilliams, 2009). Together, these equations are used to calculate the ocean state, including its velocity, salinity, temperature, and other properties as the model integrates forward in time. ROMS utilizes asynchronous time stepping, in which the effect of barotropic momentum and baroclinic momentum are not advanced at the same time, but rather using a predictor-corrector method which substantially reduces the computational cost of simulations. That ROMS is free-surface allows its output to represent the effect of surface energy dispersion which is sometimes lost in circulation models which assume a rigid lid (Shchepetkin

& McWilliams, 2009). The WAOM setup upscales ROMS to a circum-Antarctic domain and uses a curvilinear coordinate grid with a south-polar projection. The domain for WAOM (Figure 1) is rectangular and includes all of the Antarctic ice shelf cavities and the continental shelf (Richter et al., 2022).

The 10 km resolution of WAOM (WAOM10) features a 530 $\times$ 630 horizontal grid over the model domain, with depth discretized into 31 vertical layers of varying thickness, with higher resolution towards the ocean surface and seafloor. While WAOM10 is capable of permitting some large coastal polynyas (Arrigo & van Dijken, 2003) and is eddy-permitting, it is not eddy-resolving on the shallow shelves or for mesoscale eddies (Klinck & Dinniman, 2010) nor is it sufficient to represent bathymetric peaks and troughs (Dinniman et al., 2016). Recent studies using WAOM have noted slight differences between resolutions of WAOM. Richter et al. (2022) showed that average shelf temperatures in the 10 km resolution of WAOM (WAOM10) are 0.2°C warmer than the 4 km resolution (WAOM4), with additional positive biases in melt rates. Dias et al. (2023) also noted drift between the annual mean ocean heat content (OHC), mean kinetic energy (MKE), and particularly the ocean salt content (OSC) of WAOM10 and WAOM4 over time, but not within the first years of a given simulation. Despite these differences, the divergence of WMT rates near the ice shelf between the WAOM10 and WAOM4 were found to be relatively small (within 1×10^{-4} Sv difference) within Prydz Bay as compared with farther East ($\pm$ 1.5 $\times10^{-4}$ Sv). Furthermore, WMT rates on the continental shelf do not depend on WAOM resolution. This is primarily because surface forcing remains the same despite changes to model resolution. Therefore we argue that WAOM10 and WAOM4 both show realistic simulations of the study region and length of simulation of interest; the additional computational resources of running a finer resolution of the model would not show substantially different results in the trajectories of Lagrangian particles. Finally, because our study is performed over a large regional area, 10 km was deemed sufficient to create a robust dataset using the model while preserving computational efficiency.

WAOM is initialized from rest using a Repeat Year Forcing (RYF) strategy, in which the conditions of a single year (in this case 2007 which was chosen to represent a consistent normal year forcing over the full forcing data period 1992-2011) are repeated to achieve a quasi-equilibrium in the model spin-up (Richter et al., 2022). The spin-up for WAOM10 involves the application of a 20-year RYF dataset. This 20-year period should be sufficiently long to flush the sub-ice cavities (Holland, 2017) and for the ocean to reach a quasi-equilibrium state (Richter et al., 2022). WAOM does not incorporate any river runoff originating from subglacial hydrology as in Dias et al. (2023). The baroclinic model time step used is 15 minutes, with a ratio of the barotropic to baroclinic timestep of 36 to 1. The model was initialized from the final year of the two-decade spin-up, and results are analyzed using the subsequent two model years. The model was run on CSC IT Center for Science Puhti HPC using 2 x 20 core Xeon Gold 6230 processors on a total of 7 nodes.

Datasets from ECCO2 climate reanalysis were used for the lateral open boundary conditions using a Repeat Year Forcing (RYF) (Menemenlis et al., 2008). The initial conditions were derived from the ECCO2 reanalysis data from January 2007 with data extrapolated beneath the ice shelves, where sea ice buoyancy fluxes and wind stress for 2007 are non-anomalous for the period 1992–2011 (Richter et al., 2022). The seafloor topography in WAOM was derived from two sources: Bedmap2 from Fretwell et al. (2013) and RTopo-2 from Schaffer et al. (2016) for the sub-ice-shelf ocean bathymetry. WAOM uses topography smoothing in order to avoid pressure gradient errors, as is an established part of using terrain-following coordinate models.

An accurate estimation of coastal polynyas is necessary for the estimation of DSW formation which is obtained by prescribing the sea ice forcing using wind stress by using ERA-Interim 10 m wind speeds (Galton-Fenzi et al., 2012; Cougnon et al., 2013; Richter et al., 2022), and uses prescribed surface salinity and heat fluxes estimates from sea ice growth and melting derived from observations (Tamura et al., 2011). Given that polynyas are persistent sites of negative heat flux and positive salt flux during the formation of DSW, using these outputs from the model facilitates their identification and representation (Tamura et al., 2008, 2011; Cougnon et al., 2017).

Though outside our research scope, the model configuration used in this study was extended by Dias et al. (2023) further into the Ross Sea than that described in Richter et al. (2022). Furthermore, surface heat fluxes during the summer months have been reduced as compared with those used in Richter et al. (2022) to minimize SST biases. In addition, salt fluxes in this model configuration were not modified from Tamura et al. (2011) as they were in Richter et al. (2022). This ensures that salt input to the ocean remains similar to measured values, even when the model temperature in WAOM is positively biased. Ultimately, this considerably increases continental shelf bottom salinity as compared with Richter et al. (2022) to more realistic values (Dias et al., 2023).

2.2 Lagrangian Simulation and Analysis

Lagrangian diagnostics were performed using a simulation of WAOM. As with ROMS, WAOM features a built-in subroutine to perform online Lagrangian analysis. The trajectory, or flow path followed over time, of each particle in this model is modified by advective velocity and vertical diffusion (Piñones et al., 2011). The advection method WAOM uses to compute the horizontal and vertical positions of the particles is a fourth-order Milne predictor (Abramowitz & Stegun, 1964) and a fourth-order Hamming corrector scheme (Hamming, 1973), while the effect of vertical diffusion is calculated from forward differencing (Piñones et al., 2011). After these particles are released in the model, they move freely in the turbulent flow field.

An equal number of particles (amounting to 20332 total) were released weekly over the course of one model year after initializing with the 20-year RYF scheme and tracked for the subsequent year. These floats were released each week at the ocean surface at the maximal extent of the polynyas in the Prydz Bay polynya region (here defined from 60°E–85°E and above the continental shelf). Based on monthly averages of heat flux and surface salinity flux, a filter was applied so that a subset of only those 4458 particles which are both released in a seasonal polynya and which form DSW at some time in the simulation were pre-selected to calculate the results. The 328 release points for particles used in our results are shown in Figure 1. The shape and extent of these polynyas as well as whether they form DSW can vary during the Antarctic freezing period (from March to October inclusive); these seasonal changes for both named and unnamed polynyas is shown in Figure 2, where only the Darnley polynya features a late-winter signal in which more DSW is formed. In WAOM, these coastal polynyas are defined by coincidences of negative heat flux less than –120 W m^{-2} (showing surface cooling) and positive surface salinity flux greater than 1.3×10^{-5} m s^{-1} (showing brine rejection) based on results by Tamura et al. (2008) and Tamura et al. (2011). The units of salt flux are given as kg m^{-2} s^{-1} divided by the density of freshwater. Less than 1% of particles experience beaching, or stagnating on the land-ocean boundary through either ocean processes or model interpolation schemes; these were also filtered from the paper results as in Carlson et al. (2017). Finally, the number of time steps for each particle was also sliced to include only the 365 days after its initial release (trajectories of particles released in January end in January of the following year). One year was chosen as the reference frame to avoid particles experiencing two austral winters, thus increasing their likelihood of being altered by sea ice formation.

The output of the WAOM float application provides a series of particle properties recorded at each model time step. Here, the position of the Lagrangian floats changes with the local velocity and their attributes are updated every 15 minutes after their re-

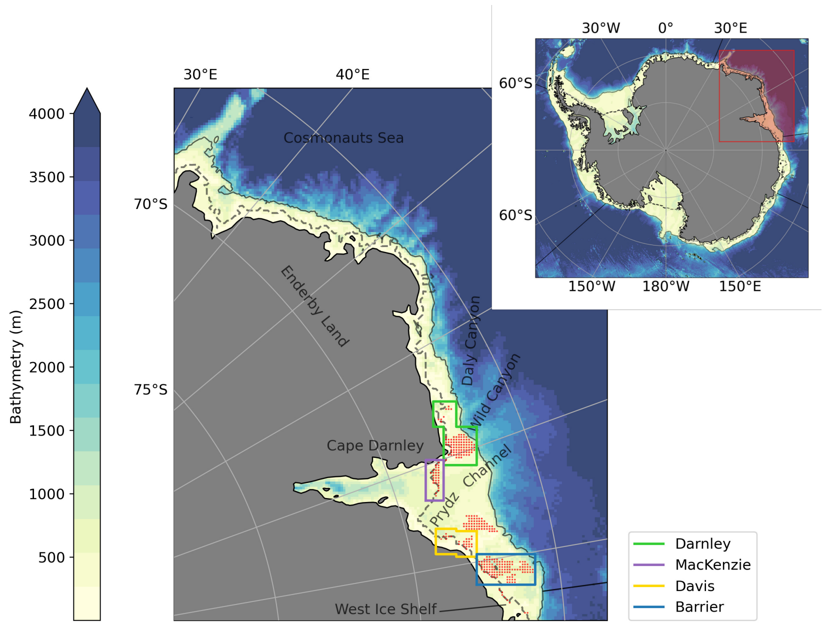

Figure 1. The maximum extent of coastal polynyas that form DSW identified by monthly averages of salt and heat flux (see Tamura et al. (2011)) during the model run. A total of 328 WAOM10 release points were used in our results. The green, purple, yellow and blue squares represent the anticipated locations of the Darnley, MacKenzie, Davis and Barrier polynyas, respectively. The ocean is colored by bathymetry represented in WAOM10, the black line represents the 1000 m isobath and location of the continental shelf break, and the grey dashed line shows the ice shelf front. Inset shows the WAOM model domain with Southern Ocean bathymetry from Richter et al. (2022).

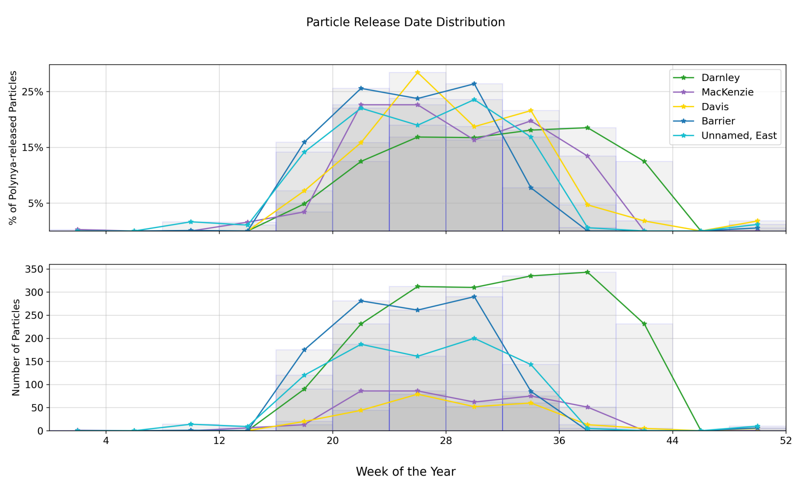

Figure 2. The seasonal distribution of polynya extent based on the mapping by Portela et al. (2022) and definitions of polynyas from Tamura et al. (2008) and Tamura et al. (2011). The first subplot shows the number of floats released in each polynya as a percentage of the total number of floats released in that polynya over time, and the second subplot shows the total number of particles released in these named and unnamed polynyas over time. Unnamed East refers to seasonal polynyas East of Prydz Bay.

lease with each baroclinic time step in the model. Properties recorded include the in situ density anomaly (σ), potential temperature (θ), practical salinity (S), depth, and coordinate positions of floats at each time step of the model run. σ in the model output is calculated with respect to the local hydrostatic pressure in order to accurately resolve horizontal pressure gradients (in units of kg m^{-3} - 1000), while potential density anomaly (σ_θ) can be calculated using absolute salinity and conservative temperature with respect to 1 bar sea surface pressure minus 1000. In this setup, particles are considered microscopic groupings of molecules without material volume. Particles record changes in heat and salt of the surrounding water. Together, the information recorded for any given particle at each time step becomes a continuous vector which we refer to as a particle trajectory (van Sebille et al., 2018). A collection of particle trajectories take a step in resolving the pathways of Southern Ocean circulation by representing the dynamics of the fluid motion and facilitating statistical analysis of flow (Malik et al., 1993).

The potential density anomaly (σ_θ) is a function of absolute salinity and conservative temperature. WMT and surface-referenced potential density anomaly (σ_θ) isopycnals represented in θ-S diagrams within our report were calculated using the non-linear Thermodynamic Equation of Seawater-2010 (TEOS-10) by Feistel (2012). Potential density in this report is referenced to sea surface pressure ($Pa = 1$ bar), reflecting the mean depth at which particles are initially released. The 75-term polynomial expression expressed by Roquet et al. (2015) was applied to the Gibbs SeaWater (GSW) Oceanographic Toolbox in order to compare WAOM output to other ocean models. In this way, GSW can be used to convert between model data (practical salinity and potential temperature), in situ observations (practical salinity and in situ temperature), and calculated location-dependent variables (absolute salinity and conservative temperature) (McDougall & Barker, 2011). Future references to "salinity" and "temperature" assume the model data variables.

Several other variables can be used to describe the processes of WMTs. First, freezing temperature (T_f) is used to define water masses on the shelf and under the ice sheet and is calculated using the absolute salinity of seawater with reference to the sea surface pressure of 1 bar (McDougall & Barker, 2011). Next, the Gade line (Gade, 1979) describes mixing between a given water mass with ice meltwater and is thus a good representation of the ISW. Our analyses also refer to this paper as the ice-ocean mixing line based on the results of McDougall et al. (2014). In Figures 3 and 5, the slope of this line is the ratio of the latent heat of freezing of seawater to the isobaric heat capacity, and practical salinity S and potential temperature θ are here chosen as $S = 34.5$ and $\theta = -2.05°C$ as characteristic values of DSW to represent mixing. As in Gade (1979), this line does not include an ice-shelf heat flux component where it is included in the model; the result is still comparable to that equation of McDougall et al. (2014) to represent glacial ice-ocean mixing. Finally, neutral density (γ) surfaces represent a multi-valued functional relation between in situ density (σ) and pressure (Stanley, 2019), and have historically been used to fit hydrographic data to density surfaces (Jackett & McDougall, 1997) and identify AABW (Orsi et al., 1999). However, because γ is a function of latitude and longitude, calculating it with select reference values becomes less accurate over large regional studies. This study utilizes primarily σ_θ as calculated from WAOM10 outputs of salinity and temperature to study WMT, which changes only as a result of mixing processes (McDougall & Barker, 2011). To verify that potential density can function for analyses in this study, key values in γ are verified using the mapping of ocean properties by Orsi and Whitworth (2005) in the location of interest and equivalent values found in σ_θ. These values are also comparable to those found in the sea ice model of Kusahara et al. (2010).

It is common practice in Lagrangian ocean analysis of residence time (Tamsitt et al., 2021; Dawson et al., 2023) and ocean currents to create binned histograms of particle pathways (Durgadoo et al., 2013; van Sebille et al., 2018). Our study includes these analyses and takes a novel approach to Lagrangian ocean analyses by applying data clustering to draw comparisons between individual particle trajectories. Hierarchical clustering for this study was performed using Ward's method to create a tree of mutually exclusive sets of particles (Ward, 1963). A KMeans algorithm was applied points in hierarchical subtrees to create clusters of particles (Pedregosa et al., 2011). Three features of individual particles were used to cluster in this study: the changes in temperature (θ), salinity (S), and in situ density (σ) between the time of particle release and one year later. The net change in particle depth was not used, even though some water masses are defined by this variable as discussed in the next section.

2.3 Water Mass Identification

One of the primary interests of this paper is to track polynya-released, DSW-forming drifters which do or do not become AABW. To complete this task as well as identify other WMTs, each particle time step is labeled and categorized as a distinct water mass. The changes to particle water mass over time are then used in the Eulerian view (see Figure 8) as a complement to analysis in the Lagrangian form. Specific rates of WMT are not quantified in this study, but rather the WMT framework is used to study key drivers of density, salinity, and temperature changes.

Several water masses can form in and around coastal polynyas including Dense Shelf Water (DSW) which can eventually form Antarctic Bottom Water (AABW). New sea ice formation in these polynyas during the winter (May through October) is associated with brine rejection, upper ocean cooling, and the formation of HSSW (Tamura et al., 2011; Ohshima et al., 2016), a transitional water mass before the critical density for DSW formation is reached. DSW is the densest water on the Antarctic shelf with a neutral density (γ) greater than 28.27 kg m^{-3} and a temperature near freezing (Portela et al., 2022). When DSW sinks beyond the continental shelf, it can mix with CDW to form AABW. Talley et al. (2011) defines AABW by its (γ) greater than 28.27 kg m^{-3}, salinity between 34.5–34.75 g kg^{-1}, and depth of greater than 1000 m. As observed in Orsi and Whitworth (2005), the top of the γ=28.27 isopycnal equivalent near Eastern Antarctica can be found where θ=–0.6°C, S=34.6; the equivalent σ_θ=27.82 kg m^{-3}. Though HSSW exists at the polynya, this water mass is not uniquely defined in this study, as its definition is so similar to other shelf waters that we refer to both water masses here as DSW (Yoon et al., 2020).

We identify several other water masses in Table 1, which have been compared with in situ observations of temperature and salinity within EN4 datasets (Good et al., 2013) as well as profiles from Ribeiro et al. (2021). These water masses near polynyas include modified Circumpolar Deep Water (mCDW), modified Shelf Water (mSW), Ice Shelf Water (ISW), and Antarctic Surface Water (AASW). mCDW can be produced through mixing across the continental shelf between waters beneath coastal polynyas and CDW which has intruded from the deep ocean onto the shelf. Next, the formation of mSW results from the mixing between mCDW and DSW. AASW can also form near coastal polynyas as a seasonally variable surface layer, with wide variations in salinity and density due to winter buoyancy loss and seasonal air-sea fluxes. (Portela et al., 2022). ISW, often located within the ice shelf cavity, has a potential θ below the surface freezing point and is composed of glacial meltwater mixed with DSW or mCDW. Finally, Winter Water (WW) can also form from the winter mixed layer and act as a temperature minimum among surface waters (Ribeiro et al., 2021). Definitions for each of these major water masses are derived from Herraiz-Borreguero et al. (2016), Herraiz-Borreguero et al. (2015), and Williams et al. (2016) as well as modified from Portela et al. (2022) so that all particle time steps can be labeled as a distinct water mass. A heatmap of the modeled particles overlayed on their definitions in θ-S space shown in Figure 3.

Table 1. Definitions of water masses by S, θ, σ_θ, and depth. Parameters used to calculate AASW, mCDW, ISW, DSW modified from Herraiz-Borreguero et al. (2016, 2015); Williams et al. (2016). HSSW defined as σ_θ>= 28 by Yoon et al. (2020) is here combined with DSW. AABW defined by Talley et al. (2011). T_f indicates the surface freezing point.

Water Mass	Name	Salinity (S)	Temperature (θ)	Density Anomaly (σ_θ)	Depth (z)
AASW	Antarctic Surface Water	$S < 34.5$	$\theta > T_f$	σ_θ< 27.73	-
mCDW	modified Circumpolar Deep Water	-	$\theta > T_f$	27.73 <σ_θ< 27.82	-
ISW	Ice Shelf Water	-	$\theta < T_f$	σ_θ< 27.82	-
DSW	Dense Shelf Water	$S > 34.5$	$\theta < T_f + 0.1$	σ_θ> 27.82	-
mSW	modified Shelf Water	$S > 34.5$	$T_f < \theta < -0.4$	σ_θ> 27.82	z >-1000
WW	Winter Water	-	$T_f < \theta < -1.5$	27.55 <σ_θ< 27.73	-
AABW	Antarctic Bottom Water	$S > 34.5$	T_f+0.1¡$\theta < 0.1$	σ_θ> 27.82	z <-1000

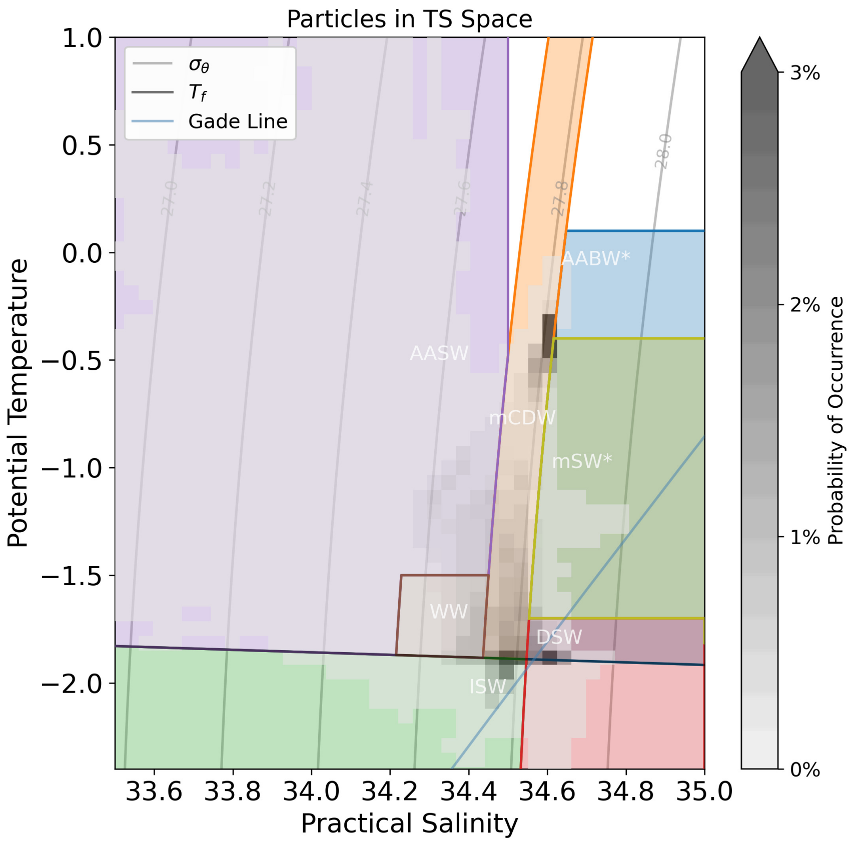

Figure 3. A binned histogram representing the most common potential temperature (θ) and practical salinity (S) values of all particles at all time steps as compared with their definitions in Table 1. The colorbar represents a heatmap of size 70 by 70 showing the probability of any one particle having any given θ-S values at any time in the model simulation. The black solid line represents the surface freezing temperature of water (T_f). The ice-ocean mixing line is also shown for interactions between ISW and DSW represented by $S = 34.5$ and $\theta = -2.05°C$. Gray solid lines represent potential density anomaly (σ_θ) and were calculated using absolute salinity and conservative temperature. Conversions to achieve model terms of salinity and temperature were performed using TEOS-10 by assuming a location within Prydz Bay (73.5089°E, -68.8245°S). Polygons in the figure show labeled relevant water masses. Water masses labeled with an asterisk are also defined by particle depth.

Lagrangian particles are not assumed to have any volume unless the continuum hypothesis is made and the transport is defined by the instantaneous velocity of a particle multiplied by the size of its model grid cell van Sebille et al. (2018). In our study, we note that particles are only released in select coastal polynyas, not along broad swathes of the coast. For this reason, calculating volume transport would not be comparable to similar studies on the region (e.g., Li et al. (2023); Gunn et al. (2023)). Estimates for WMT are instead considered only by their ratios to one another rather than their discrete volume.

3 Results

3.1 Distribution and Timescales

3.1.1 Probability Distribution

We begin by taking a probabilistic approach to the distribution of all particles released in polynyas to outline the currents which transport these Lagrangian particles. A binned histogram in Figure 4a shows the probability that any given particle will appear at least once during the year after their release. Here, each WAOM10 grid cell is colored by the sum of independent observations within that map area normalized by the total number of particles released and given as a percentage.

The dominant flow of particles from Prydz Bay is westward along the ASC and at the edge of the continental shelf. Of those less than 1% of particles recirculate East through a cyclonic gyre in Prydz Bay, most are bounded by the presence the West Ice Shelf (see Figure 4). Two trajectories appear outwards from the bay: one along the Prydz Channel (11% likelihood) and the other just next to Cape Darnley (7% likelihood). Downstream, these trajectories merge West of Cape Darnley, where particles are up to 43% likely to appear along the ASC. Particles continue along the ASC with up to 14% passing westward of the 50°E vertical. In addition to this dominant pathway approximately above the 1000 m isobath, several secondary pathways exist by which particles leave the continental shelf. Few particles flow through the Wild Canyon and they are up to 5% likely to flow through the Daly Canyon off the shelf break. West of the 50°E, particles may follow several smaller canyons to depart to the continental shelf. Importantly, fewer than 5% of the particles leave the continental shelf from Prydz Channel directly; this departure occurs primarily downstream of Cape Darnley. Westward flow plotted here highlights the importance of the ASC in carrying particles to AABW pathways and is consistent with Thompson et al. (2018)'s characterization of Prydz Bay as having few shelf overflows.

3.1.2 Residence Time

The residence time of the particles can also be visually represented in binned histograms. Residence time is defined as the transit time of any given particle passing through a WAOM10 grid cell (van Sebille et al., 2018). Calculating residence time for all Lagrangian particles across bins of the native grid thus yields multiple times for each WAOM10 square. In Figures 4b and 4c, the mean and standard deviation of particle residence times are shown for bins through which at least 5 particles pass during the model time frame to show the range of timescales by which currents transport particles (Rühs et al., 2013). The resulting mean residence times of all particles in one WAOM10 grid square (Figure 4b) can range up to 26 days. The highest mean residence times of particles are both under the Amery Ice Shelf and beyond the continental shelf break, while the mean residence time along the continental shelf break is typically less than 5 days for any WAOM10 grid cell. Figure 4c shows the greatest variances in residence time exist both on the shelf near the Amery Ice Shelf edge as well as off the shelf in the deep ocean.

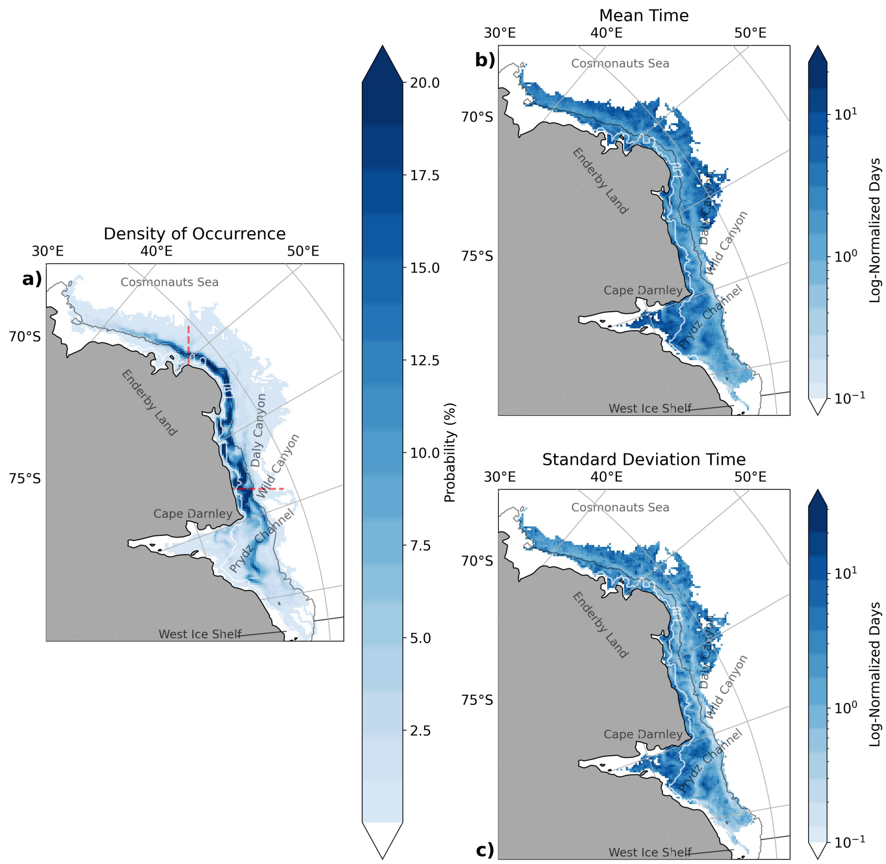

Figure 4. (a) a histogram representing the probability (from 0 to 100%) that a Lagrangian particle appears at least once in any WAOM10 grid cell in the year after its release. Red dashed lines in (a) define the sections used in Figure 9 and the Discussion section. Histograms on the right show (b) the log-scaled variation of mean residence times within WAOM10 grid squares with at least 5 particles, and (c) the log-scaled standard deviation of residence time within WAOM10 grid squares with at least 5 particles. (a)-(c) feature light gray lines as the latitude and longitude of the map area, and a darker gray line shows the 1000 m isobath around the continent. The edge of the ice shelf is marked as a white line. Major topographic features are labeled.

The minima in particle residence times in Figures 4b and 4c are nearly an opposite reflection of the maxima in 4a, highlighting both the speed and strength of the ASC in East Antarctica as described by Nunes Vaz and Lennon (1996). Furthermore, this westward pathway could have implications for how water masses are redistributed toward the deep ocean. For instance, water sourced from coastal polynyas that is carried along the ASC may interact with downstream ice shelves or upwelling CDW, thus altering its likelihood to sink to bottom water pathways.

3.2 Trajectory Clustering

3.2.1 Size and variation of clusters

Clustering particles help parse individual trajectories, whose wide range of values is identified in Figure 4. Here, four clusters of drifters were created, each with at least some particles released from March through October inclusive; four is a small enough number of groups to manage and visualize, yet large enough to represent differences between water mass transformations and differentiate AABW-forming particles. Other numbers of clusters were tested, but four was found to be the best for this study's purposes, and null hypothesis significance testing performed by a Kolmogorov-Smirnov algorithm was done to ensure data were not drawn from the same distribution. Figure 5 shows each of these clusters as a 70 by 70 gridded heatmap in θ-S space (fine enough to represent major features and mixing), with the same polygons representing water mass as in Figure 3.

A clear distinction is identified in the temperature and salinity values change for the four clusters. First, Groups 1 and 2 show interactions along the glacial ice-ocean mixing line (Gade, 1979; McDougall et al., 2014), indicating the formation of ISW, whereas no similar pattern appears in Groups 3 and 4. Furthermore, the ending points in the former two clusters are fresher than those in the latter. Particularly in Group 1, the range of θ-S values at the end of the simulation is far greater than in any other group, which suggests that interactions with the ice shelf can induce buoyancy gain in polynya-sourced water. The next observable difference appears in how particles appear to mix. In Groups 3 and 4, aggregations of starting points appear just above the surface freezing temperature and ending points appear AABW, a feature which suggests these clusters mix along the isopycnals rather than across them. We note here that temperature and salinity values can change either from advection across isopycnals or as a result of local variability in the surrounding water (Groeskamp et al., 2014). However, the lack of trajectories within the AASW regions of these θ-S plots confirm that the mixing in these latter two groups does not occur across isopycnals to the same extent as in Groups 1 and 2.

3.2.2 Mixing and density distribution

The changes to particle depth can also be visualized in comparison to time and density, as shown in Figures 6 and 7, respectively. The rate of particle sinking and associated buoyancy losses vary quite substantially between the clusters. As in Figure 6, particles in Group 2 sink quite rapidly, losing buoyancy and remaining at depth after they sink to the ocean floor. Group 2 also sinks past the continental shelf but does not sink as deep as the latter two groups (1000–3000 m for Group 2 as compared with 1500+ m for Groups 3 and 4). Particles in all groups are not static in depth; they tend to sink and experience upwelling several times, which might result from convection. Conversely, particles within Group 1 remain close to the surface throughout the year. The noted convection, or sinking and resurfacing of some particles, might result from shoreward intrusions of CDW onto the shelf where isopycnals tilt towards the continental shelf (Thompson et al., 2018), keeping these particles relatively warm and shallow. For Groups 2-4, no specific days—which might represent notable weather events—were correlated with sinking particles.

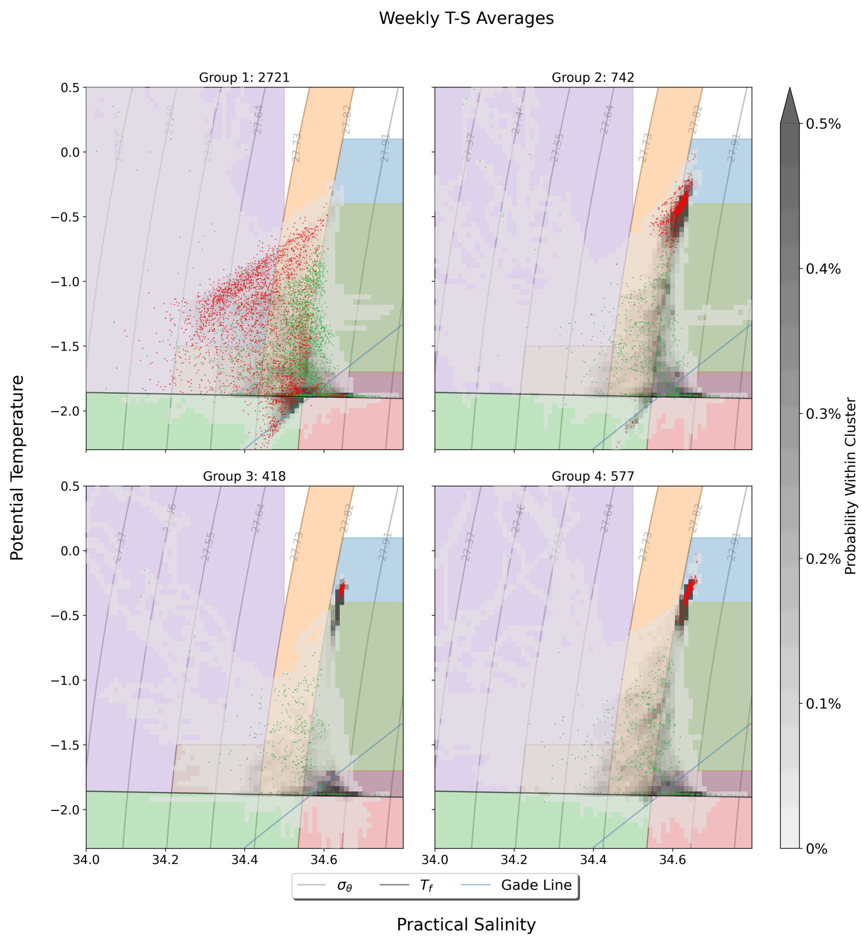

Figure 5. Heatmaps of resolution 70 by 70 showing each of the θ-S values for each of the four clusters of particles, with the number of particles per cluster listed in the title. Water mass definitions are marked by polygons as in Figure 3, the glacial ice-ocean mixing line marked in blue, T_f demarcates the sea surface freezing temperature, and σ_θ marks the potential density anomaly isopycnals. The θ-S values at the time of release for each particle is marked in green, and those values after one year of the model run are marked in red.

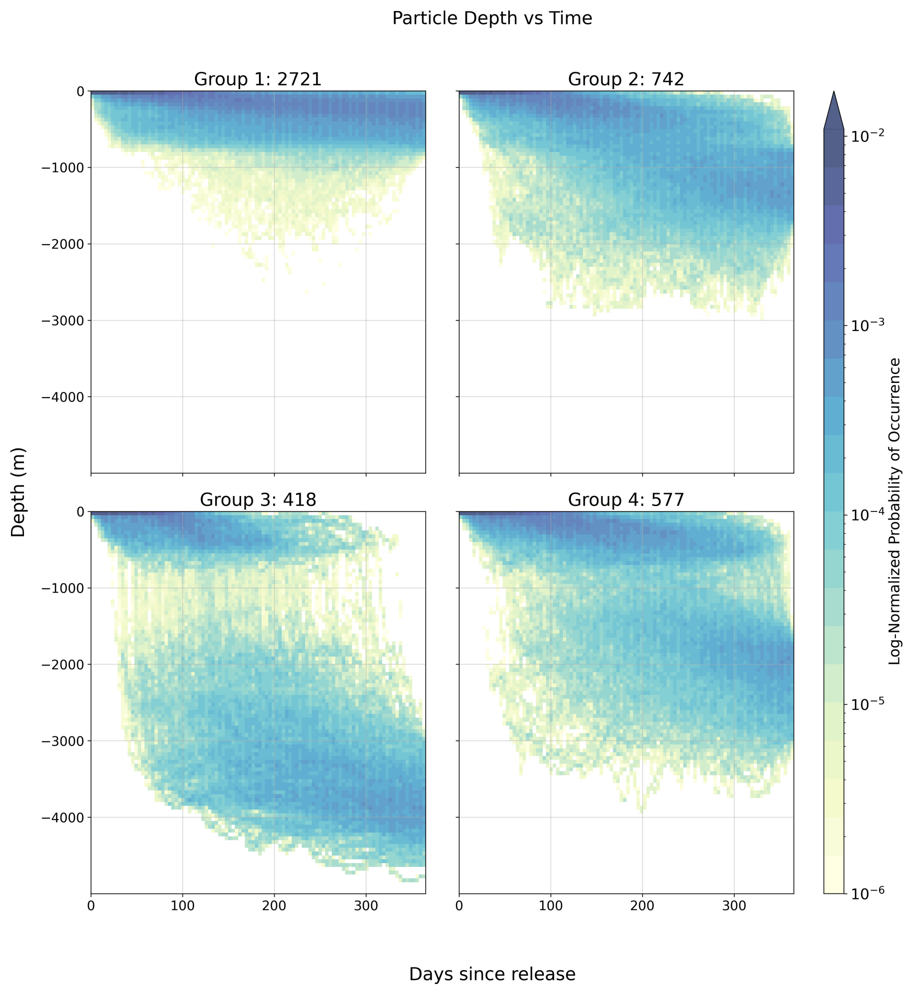

Figure 6. The changes to particle depth (m) over time of the clusters. The trajectories of particles in each subfigure correspond to particles within that cluster, and the number of particles in each cluster is labeled at the top of the figure. Data points are colored by the density of particles in the depth-time space.

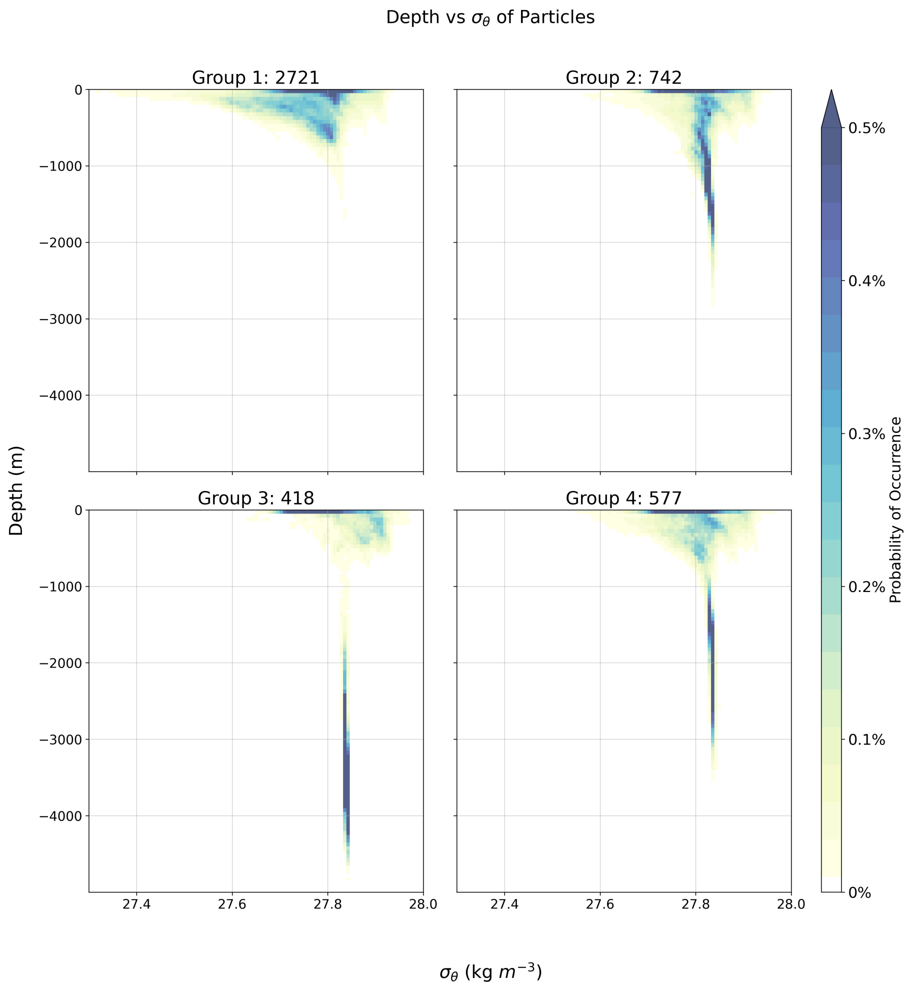

Figure 7. A figure showing the changes to depth (m) over sea surface pressure-referenced potential density anomaly (σ_θ) of different clusters. The trajectories of particles in each cluster are shown in the subfigures with the number of particles shown at the top. Particles are colored by the number of days since their release. Most changes to density occur above 1000 m depth.

The changes to density with depth of the clusters in Figure 7 also reveal that buoyancy changes occur primarily in the upper ocean. For the AABW-forming Groups 3 and 4, particles sink to reach a fixed density, which does not change once it is reached. Thus, these particles describe well the basic process of bottom water formation within the lower limb of Southern Ocean overturning. However, if these particles are found at the upper edge of the bottom water, shearing with CDW may be inducing eddy formation, causing these particles to fluctuate in depth after they initially sink. Nearer to the surface, greater variability in density is possible. For Group 2 specifically in which many of the particles return to depths above 1000 m, the combined effect of upwelling and convection may be reflected. At the surface, Group 1 features the most variability in density with time due to surface interactions. Groups 1 and 2 likely characterize the upper limb of the Southern Ocean overturning, or are not taking a part of it at all.

3.3 Water Mass Transformations

The released particles can be plotted in θ-S space, and their definitions as water masses over time can be defined by Table 1. The variations of particles in θ-S space is noted with the definitions for water masses in Figure 3. Here, the S and θ values for all particles at all time steps are used to create a 70 by 70 binned histogram—fine enough to resolve notable features—between the maximum and minimum values for salinity and temperature appearing in the simulation. The probability of any given pair of temperature and salinity values appearing at any time in the simulation was then used to create this histogram or density map, which demonstrates key locations of water mass transformation in θ-S space. In Figure 8, the definitions for AABW and mSW are also defined by depth. While AASW features the largest variation in temperature and salinity, the most common water mass to appear at any given time step is mCDW. At any time step during the one-year simulation, most particles fall between the σ_θ isopycnals of 27.6 to 27.9 kg m^{-3}; the WMTs among these high-density waters are the most important to understand the coastal processes near Prydz Bay.

The number of particles that form AABW can depend on the starting water mass. To show this and some notable differences between the clusters, the distribution of water masses at the start and end of the model simulation are shown in Table 2. For Group 1, none of which becomes bottom water, more particles were released at the beginning of the study as WW and AASW, and less comparatively as DSW than the other groups. Groups 1 and 2 are the only clusters in which particles are released cold and fresh enough to be categorized as ISW; these are also the only groups where particles end as ISW at the end of the study. With higher comparable portions of particles starting as DSW, particles in Groups 3 and 4 all end as AABW by one model year after their release.

To investigate where WMTs occur in relation to the bottom topography and continental shelf, we shift to an Eulerian view of the simulation results in Figure 8. Here, particles' coordinate location at each time step is colored by their respective water mass label, overlaid on a bathymetric map.

Water masses on the shelf and within Prydz Bay itself feature similar trends among the groups. The densest water mass on the shelf, DSW, typically appears near Cape Darnley in all cases before it is advected downstream and transformed. mSW is also advected by the ASC towards the West and appears both within Prydz Bay or beyond it on the continental shelf. One common WMT for both of these water masses is the transition to mCDW which occurs due to interactions with intruding CDW and warming on the shelf. For DSW the transformation to mCDW (or first mSW) occurs only within 72–76°E, while for mSW it occurs at any point East of the Enderby projection. mCDW then can be transported either along the ASC or beyond the continental shelf break. Of the less-frequently appearing water masses, WW can also appear at any location but is most fre-

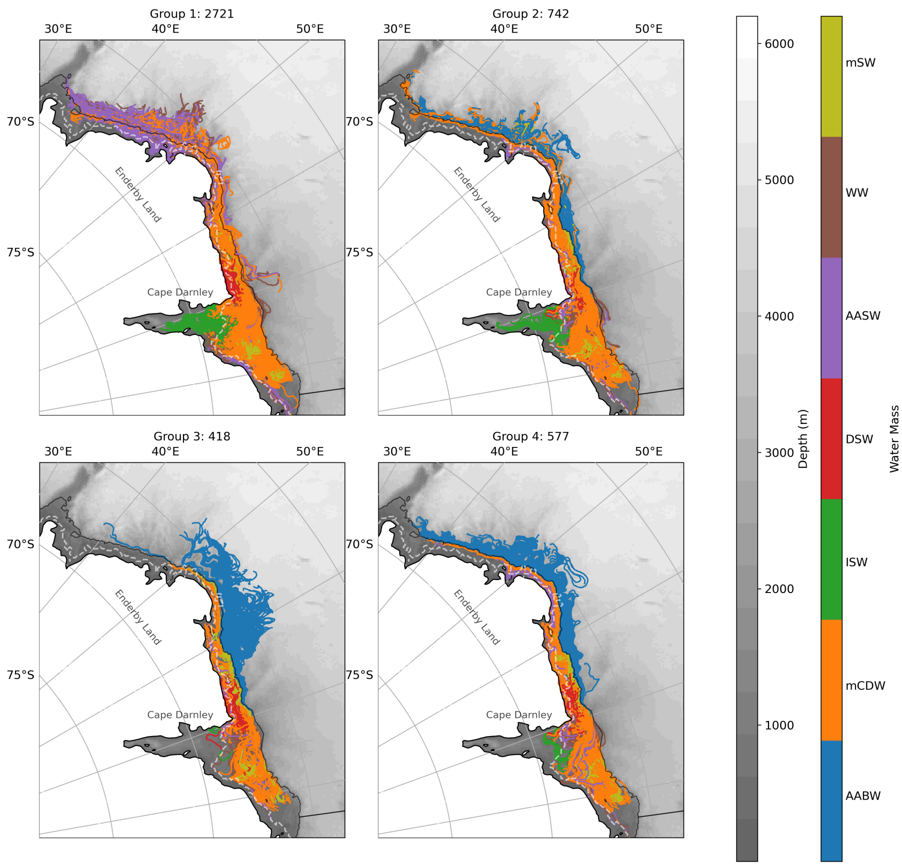

Figure 8. Clustered particle trajectories in geographical space. The trajectories are colored by their definition in Table 1. Trajectories shown are over the course of one year, and the number of particles in each group is shown in the title of the plot. The background shows model bathymetry, and the solid and dashed lines represent the continental shelf break and the edge of the ice shelf, respectively.

Table 2. A table describing the starting and ending points for trajectories in each of the four clusters. The relative sizes of the clusters are shown. The percentage of points in each water mass is also given at both the start and the end of the model simulation. Water masses are identified by their definitions in Table 1.

Time	Group	% of Total	AABW	mCDW	ISW	DSW	AASW	WW	mSW
Start	1	61%	0%	50%	1%	25%	6%	5%	13%
	2	17%	0%	47%	1%	31%	6%	3%	12%
	3	9%	0%	50%	0%	30%	6%	3%	11%
	4	13%	0%	46%	0%	30%	6%	6%	12%
End	1	61%	0%	37%	9%	3%	42%	8%	1%
	2	17%	60%	36%	2%	0%	0%	0%	2%
	3	9%	100%	0%	0%	0%	0%	0%	0%
	4	13%	100%	0%	0%	0%	0%	0%	0%

quent at the edges of the Amery Ice Shelf, while AASW appears with the most frequency West of the Enderby Land projection in Group 1.

An interesting result of this kind of analysis is in the demonstrated interactions between particles and the Amery Ice Shelf. As similarly noted in section 3.2.1, Groups 1 and 2 clearly form ISW in Figures 5 and 8 where Groups 3 and 4 do not. The freshening demonstrated in Group 1 by the formation of mCDW and AASW with the exclusion of any AABW formation demonstrates that interactions with the ice shelf induce buoyancy gain among particles. Even in Group 2 which forms some bottom water, the formation of ISW appears to enrich particles with freshwater even after they are advected westward; only some of these floats still sink to the ocean's abyss. As noted in Figure 7, AABW in this group also end at a shallower depth in Group 2 as compared with Group 3. That the ice shelf meltwater precludes or at least limits the formation of AABW is a key process, and particle residence time under the ice shelf should be studied further to quantify the implications of WMT at the edge of the Amery Ice Shelf.

4 Discussion

We argue that the four clusters represent two of the three cases of ASC transport as described by Thompson et al. (2018). Group 1 represents what Thompson et al. (2018) describes as the "fresh shelf case", in which CDW intrudes onto the shelf to keep dense waters near the surface and density isopycnals slope downwards towards the continental shelf break. Groups 3 and 4 represent a "dense shelf case" where dense water sink below intrusions of CDW to the abyssal plane, and density isopycnals follow the continental slope. Group 2 here represents a transitional scenario between the two, in which initial modification under the ice shelf leads to the formation of fresher bottom water. Rather than numbers, the four clusters will be referred to by their physical characteristics for the remainder of our discussion. We demonstrate these cases by showing two transects in Figure 9. At Cape Darnley at 68°, isopycnals tilt parallel to the continental shelf, and the temperature profile has a V-shape with colder temperatures at the sea surface and seafloor, characterizing the "dense shelf" along which DSW is exported. Contrastingly, beyond the Enderby Land at 50°, σ_θ isopycnals are roughly perpendicular to the continental slope, and the temperature contours tilt downwards towards the shelf, indicating a "fresh shelf" which prevents denser waters from sinking.

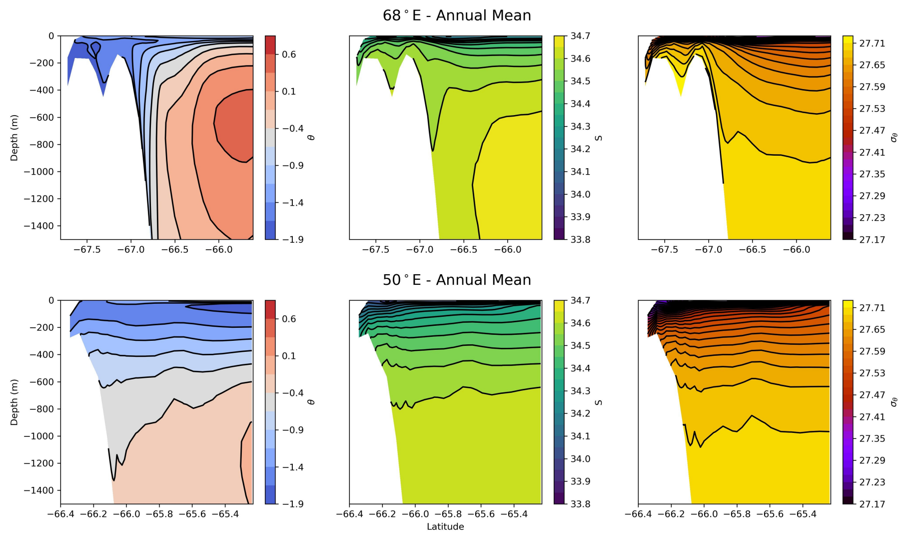

Figure 9. Sections from two transects (shown in Figure 4) displaying the annual mean of the vertical temperature, salinity, and σ_θ anomaly profiles in a "dense shelf case" (at 68°) and in a "fresh shelf case" (at 50°).

4.1 Sensitivity of AABW Formation to WMT, Topography, and Mixing Processes

4.1.1 Eulerian Water Mass Transformation

Our results suggest that particles in the fresh and intermediate clusters (Groups 1 and 2) which do not form AABW within one model year, have gained buoyancy due to meltwater beneath the Amery Ice Shelf (Figure 5, panels on the top include particles on the Gade line; Figure 8; panels on top include green trajectories). These particles initially form ISW on the shelf, and through further mixing with surrounding water masses, contribute to the formation of intermediate water masses such as AASW and mCDW rather than AABW. Thus, the formation of ISW and its freshening from melting and refreezing under the ice shelf can prevent the formation of AABW later on. Several studies have noted the suppressing factor of ice meltwater on Southern Ocean overturning and particularly its effect on AABW formation (Pellichero et al., 2018; Aguiar et al., 2023), which can occur in Prydz Bay after advection of shelf water under the ice shelf inducing basal melting (Liu et al., 2017; Jacobs et al., 1992). Once these sub-ice shelf waters are enriched with freshwater, they can leave the ice shelf again, mixing with surface waters or CDW to warm and form WW or mCDW. However, the previous influence of ice shelf meltwater makes for a more buoyant AABW, as is found by Li et al. (2023). Our results not only confirm that Antarctic ice melt can drive bottom water freshening but also underscore that these freshwater fluxes can limit DSW export from polynyas which may otherwise have formed AABW.

Interactions between CDW, DSW, and AASW also have an observable effect on AABW formation. In Figure 5, the fresh shelf case features more extensive modification in the AASW and mCDW quadrants in θ-S and less in the DSW quadrant than the intermediate case; these fresh shelf particles ultimately remain near the surface (Figure 6). This difference is not noted in Figure 8, where all clusters show the presence of mCDW at some time on the shelf. These results provide an example of how the intrusions of CDW can play a key factor in determining whether shelf water can sink toward the deep ocean. This dynamic is consistent with the studies of the region: previous literature has documented shoreward heat transport by upwelled CDW in the Prydz Bay region (Guo et al., 2019), inducing ice shelf melt and buoyancy forcing on the shelf (Liu et al., 2017) and limiting the export of DSW to the deep ocean (Morrison et al., 2020; Portela et al., 2022). Our results support that these intrusions can limit AABW formation. We also speculate that a longer simulation could show further interactions between these shelf waters and seasonal polynyas in seasonal cycles.

4.1.2 Influence of Bed Topography

Bed topography has a notable influence on the export of shelf water in the intermediate and dense shelf cases, but not the fresh shelf case. In Figure 8, particles destined to form AABW preferentially sink in subsea troughs, including Prydz Channel and the Daly and Wild Canyons; the transformation from mCDW or mSW to AABW (orange or olive to blue) also occurs at the shelf break. Furthermore, those intermediate case particles both travel farther along the shelf (Figure 8) and sink to shallower depths (Figure 6) than the dense shelf cases. The results of the intermediate case may reflect the shallower slope found downstream of Prydz Bay as compared with near Cape Darnley, as well as suggest that more modification on the continental shelf can lead to freshening of AABW. These analyses underscore the importance of steeper submarine valleys as sites of DSW transformation to AABW and agree with previous studies that topography is important to the export of dense water, both at Prydz Bay and Cape Darnley (Portela et al., 2022; Baines & Condie, 1985), likely by influencing the strength of the ASC and cross-slope flow (Thompson et al., 2018). However, because ROMS uses bottom topography smoothing to avoid pressure gradient errors, downslope flows may be represented differently here than when using a z-level model (Richter et al., 2022). Further study should include a comparison of WAOM to other ocean models to reproduce different representations of AABW interaction with the seafloor.

The extent to which the seafloor affects WMTs likely reflects the resolution of the model. While uniform grid spacing of 10 km is "eddy-permitting" as discussed in section 2, Klinck and Dinniman (2010) suggests changes to bottom topography resulting from alterations to horizontal resolution could strengthen circumpolar currents and alter exchanges of heat across the shelf break. The findings by Dias et al. (2023) agree that WAOM4 shows a stronger bottom-intensified ASC than the courser resolution WAOM10. Thus, using WAOM10 likely increases the residence time along the trajectory of the ASC as compared with WAOM4. Dias et al. (2023) also notes that using a courser topography is associated with greater buoyancy loss (up to 3 Sv difference in WMT rates) for higher densities ($\sigma_\theta > 27.6$ kg m^{-3}). Because increased residence time on the shelf is associated with the formation of more buoyant waters in our study, we argue that the effect of this buoyancy loss in WAOM10 is somewhat compensated by the weakened ASC, and the coarser resolution provides comparable results to a study performed with WAOM4.

4.1.3 Changes in Temperature and Salinity

We further investigate the roles of diapycnal and isopycnal mixing by identifying the changes to the four clusters in θ-S space using Figure 5. In the fresh shelf cases, diapycnal mixing facilitated by Ekman transport creates a larger range of θ-S both during and at the end of the simulation. Despite that all groups have a similar spread of starting points in θ-S space, there is a clear migration to lower density classes in this fresh case, whereas this does not occur in the other three panels. Along-isopycnal mixing in the two dense shelf cases is responsible for most of the formation of AABW (Figure 5 bottom panels). In these cases, a clear path from DSW to AABW ending points emerges as particles subduct along the σ_θ isopycnals; in their tractories, these particles may be AASW only briefly before sinking to the ocean floor. The lower panels of Figure 7 confirm that these dense shelf case particles only alter their buoyancy on the shelf, reflecting the downward-sloping isopycnals along the continental shelf. The vertical stratification required to allow for these dense outflows on the seafloor is enabled by shoaling of CDW above these particles (Baines & Condie, 1985; Gill, 1973; Thompson et al., 2018), which alters the temperature of dense flows but not their salinity or density. It is also interesting to note that, in contrast to many overflows in the northern hemisphere (such as in the Denmark Strait, or the Arctic shelves), due to the upward-sloping isopycnals the descending plume flows in waters that are close to its own density and thus there is little entrainment to plume.

A combination of two patterns of mixing—along isopycnals or across them—can drive coastal waters to form more buoyant, fresher AABW. In the intermediate case as identified in Figure 5, even for particles that begin as DSW, diapycnal mixing with other surface waters including ISW can increase buoyancy when water is advected under the ice shelf by means of shoaling of other water masses from offshore. However, unlike the fresh shelf case, this water can still lose buoyancy through interactions with coastal polynyas after its initial release, forming mCDW and then lighter AABW by sinking along density isopycnals (Thompson et al., 2018).

4.2 Comparison to Observational and Model Results

We compare the results from WAOM on dense water export and WMT to other studies using in situ observations. Our study highlights two pathways as key in connecting coastal polynya-sourced DSW to AABW export: the Prydz Channel and Cape Darnley (Figures 4 and 8), consistent with the results from elephant seal data by Portela et al. (2022) as well as oxygen isotope samples by Jia et al. (2022). Lagrangian analyses with WAOM also note the Wild and Daly canyons as important export pathways for AABW; Ohshima et al. (2013)'s utilization of seal data confirms the same result. Next, the inverse correlation between interactions with the Amery Ice Shelf cavity in this study (green trajectories in Figure 8 and interactions along the Gade line in Figure 5) is qualitatively in line with seal data studies showing basal melt as a limiting factor for DSW production in MacKenzie polynya (Portela et al., 2021). Additionally, the results of WMT in Table 2 show quantitative agreement with in situ observations from Pellichero et al. (2018). We show 26% of particles form AABW as compared with 19% of upwelled CDW entering the lower limb of the MOC; our study also shows a greater proportion of exported water becoming mCDW rather than surface waters in the noted study. While these results should not be directly compared—the methodology of Pellichero et al. (2018) does not accurately resolve polynyas—that these results are consistent underscore this region as a site of substantial bottom water formation requiring further study to quantify its influences on the MOC.

In our study, the shelf residence times of Lagrangian particles (Figures 4b and 4c) are remarkably similar to those of floats released at 1000 m depth using MOM01 by Tamsitt et al. (2021). However, average residence times in MOM01 are up to 50 days greater beneath the Amery Ice Shelf than in our WAOM10 study. We speculate this difference results from the coarser model resolution used in our study as compared with a zonal resolution of 2.6–5.5 km in that of Tamsitt et al. (2021). Figure 4a in our results is also quantitatively similar to the representation of the ASC using ACCESS-OM2-01 Lagrangian particles (Dawson et al., 2023) as well as abyssal transport of AABW using passive tracers (Solodoch et al., 2022).

Next, we contrast the distribution of particles in the WMT framework in WAOM10 with the results of other ocean models. After one year, our study found a ratio of 5 particles with $\sigma_\theta > 27.8$ kg m^{-3} and depth above 2000 m for every 3 particles with $\sigma_\theta > 27.8$ kg m^{-3} and depth below 2000 m. Comparing this with the results after 25 years from passive tracers released in Prydz Bay and Cape Darnley using the CCSR Ocean Component Model (COCO), Kusahara et al. (2017) found this ratio to be 1 volume of water in the former category for every 2 in the latter. The discrepancy in the formation of water $\sigma_\theta > 27.8$ kg m^{-3} between our study and that of Kusahara et al. (2017) may result from the difference in the length of the simulation (1 year in our study vs 25 in Kusahara et al. (2017)). This difference may have also resulted from the representation of polynyas with WAOM. The results of our study also show similarities with Li et al. (2023), in which meltwater from the continent and the formation of ISW led to a contraction of AABW formation using ACCESS-OM2-01. However, Li et al. (2023) describes this shift as a result of descending isopycnals (rather than buoyancy forcing by the meltwater itself). While our study does not comment on changes to isopycnals along the shelf, the results agree that the influence of ISW can either prevent bottom water formation entirely or form more buoyant AABW.

5 Conclusions

We used virtual Lagrangian floats within the WAOM10 ocean model to examine the influences of WMT, seasonality, local topography, and various forms of ocean mixing on AABW formation and export from the Prydz Bay and Cape Darnley polynya regions. Cluster analysis was used to find four unique trajectories of water mass transport from the Prydz Bay polynyas to the deep ocean. Our study offers a novel viewpoint on the AABW formation in Eastern Antarctic by combining Lagrangian trajectory analysis with water mass transformation framework. However, the study is somewhat idealized and many aspects could be further expanded on. For example, here we did not calculate volume transports but rather used comparative analysis to analyze the importance of the identified water mass pathways. Furthermore, the results are based on simulations with single year forcing and does not account for the impact of climate variability. Thus, our study does not fully quantify the impact of various processes on polynya-influenced WMT but rather builds a qualitative understanding on their roles in AABW formation.

Despite the various shortcomings of the study, the results offer a detailed view of the complex dynamics of AABW formation from Prydz Bay. Of the Lagrangian particles released in Prydz Bay coastal polynyas, 26% become AABW within one year. Our results suggest that mixing between crucial water masses, mCDW, and particularly ISW, reduces the conversion of DSW to AABW. The ultimate formation of AASW or mCDW, or some more buoyant forms of AABW is associated with longer residence time on the continental shelf and more interactions in the mixed layer, diapycnal mixing, and interactions with the ice shelf meltwater. In agreement with previous studies, we find that DSW export takes place along local canyons. Expanding on previous studies of this region, our study suggests probable implications for AABW formation under increasing ice shelf meltwater production under climate warming scenarios. We suggest that, even if the current processes of DSW production in coastal polynyas would not change in the future, mixing with ambient waters on the shelf that are becoming warmer and fresher, including ISW and CDW, will change the strength of AABW formation. Paired with anticipated changes to CDW upwelling in the coming decades, further study on Prydz Bay and Amery Ice Shelf interaction is imperative to understand the controls on AABW formation in this critical region.

Open Research Section

Upon publication, the key model fields and the Lagrangian trajectories will be made available through CSC's FAIR data platform (https://www.fairdata.fi/) and the model code, as well as analysis scripts, will be distributed using https://zenodo.org/.

Acknowledgments

This has been funded by the Academy of Finland and the COLD project. Margaret Murakami was supported by the Academy of Finland (project 322432), and Petteri Uotila by the European Union's Horizon 2020 research and innovation framework programme (PolarRES project grant no. 101003590).

References

Abernathey, R., Gnanadesikan, A., Pradal, M.-A., & Sundermeyer, M. A. (2022). Chapter 9 - isopycnal mixing. In M. Meredith & A. Naveira Garabato (Eds.), *Ocean mixing* (p. 215-256). Elsevier. Retrieved from `https://www.sciencedirect.com/science/article/pii/B9780128215128000165` doi: https://doi.org/10.1016/B978-0-12-821512-8.00016-5

Abernathey, R. P., Cerovecki, I., Holland, P. R., Newsom, E., Mazloff, M., & Talley, L. D. (2016, August). Water-mass transformation by sea ice in the upper branch of the Southern Ocean overturning. *Nature Geoscience*, *9*(8), 596-601. doi: 10.1038/ngeo2749

Abramowitz, M., & Stegun, I. A. (1964). Handbook of mathematical functions with formulas, graphs, and mathematical tables. In (Vol. 55, p. 1046). Dover Publications.

Aguiar, W., Lee, S.-K., Lopez, H., Dong, S., Seroussi, H., Jones, D. C., & Morrison, A. K. (2023). Antarctic bottom water sensitivity to spatio-temporal variations in antarctic meltwater fluxes. *Geophysical Research Letters*, *50*(13), e2022GL101595. Retrieved from `https://agupubs.onlinelibrary.wiley.com/doi/abs/10.1029/2022GL101595` (e2022GL101595 2022GL101595) doi: https://doi.org/10.1029/2022GL101595

Amblas, D., & Dowdeswell, J. (2018). Physiographic influences on dense shelf-water cascading down the antarctic continental slope. *Earth-Science Reviews*, *185(August)*, 887-900. doi: 10.1016/j.earscirev.2018.07.014

Anilkumar, N., Jena, B., George, J. V., P, S., S, K., & Ravichandran, M. (2021). Recent freshening, warming, and contraction of the antarctic bottom water in the indian sector of the southern ocean. *Frontiers in Marine Science*, *8*. Retrieved from `https://www.frontiersin.org/articles/10.3389/fmars.2021.730630` doi: 10.3389/fmars.2021.730630

Arrigo, K. R., & van Dijken, G. L. (2003). Phytoplankton dynamics within 37 antarctic coastal polynya systems. *Journal of Geophysical Research: Oceans*, *108*(C8), 18. Retrieved from `https://agupubs.onlinelibrary.wiley.com/doi/abs/10.1029/2002JC001739` doi: 10.1029/2002JC001739

Baines, P. G., & Condie, S. (1985). Observations and modelling of antarctic downslope flows: A review. In *Ocean, ice, and atmosphere: Interactions at the antarctic continental margin* (p. 29-49). American Geophysical Union (AGU). Retrieved from `https://agupubs.onlinelibrary.wiley.com/doi/abs/10.1029/AR075p0029` doi: https://doi.org/10.1029/AR075p0029

Carlson, D. F., Suaria, G., Aliani, S., Fredj, E., Fortibuoni, T., Griffa, A., … Melli, V. (2017). Combining litter observations with a regional ocean model to identify sources and sinks of floating debris in a semi-enclosed basin: The adriatic sea. *Frontiers in Marine Science*, *4*. Retrieved from `https://www.frontiersin.org/articles/10.3389/fmars.2017.00078` doi: 10.3389/fmars.2017.00078

Cougnon, E. A., Galton-Fenzi, B. K., Meijers, A. J. S., & Legrésy, B. (2013). Modeling interannual dense shelf water export in the region of the mertz glacier tongue (1992–2007). *Journal of Geophysical Research: Oceans*, *118*(10), 5858-5872. Retrieved from `https://agupubs.onlinelibrary.wiley.com/doi/abs/10.1002/2013JC008790` doi: https://doi.org/10.1002/2013JC008790

Cougnon, E. A., Galton-Fenzi, B. K., Rintoul, S. R., Legrésy, B., Williams, G. D., Fraser, A. D., & Hunter, J. R. (2017). Regional changes in icescape impact shelf circulation and basal melting. *Geophysical Research Letters*, *44*(22), 11,519-11,527. Retrieved from `https://agupubs.onlinelibrary.wiley.com/doi/abs/10.1002/2017GL074943` doi: https://doi.org/10.1002/2017GL074943

Dawson, H. R. S., Morrison, A. K., England, M. H., & Tamsitt, V. (2023). Pathways and timescales of connectivity around the antarctic continental shelf. *Journal of Geophysical Research: Oceans*, *128*(2), e2022JC018962. Retrieved from `https://agupubs.onlinelibrary.wiley.com/doi/abs/10.1029/2022JC018962` (e2022JC018962 2022JC018962) doi: 10.1029/2022JC018962

Dias, F. B., Rintoul, S. R., Richter, O., Galton-Fenzi, B. K., Zika, J. D., Pellichero, V., & Uotila, P. (2023). Sensitivity of simulated water mass transformation on the antarctic shelf to tides, topography and model resolution. *Frontiers in Marine Science*, *10*. Retrieved from `https://www.frontiersin.org/articles/10.3389/fmars.2023.1027704` doi: 10.3389/fmars.2023.1027704

Dinniman, M. S., Asay-Davis, X., Galton-Fenzi, B., Holland, P., Jenkins, A., & Timmermann, R. (2016, 12). Modeling ice shelf/ocean interaction in antarctica: A review. *Oceanography*, *29*, 144-153. doi: 10.5670/oceanog.2016.106

Dinniman, M. S., Klinck, J. M., & Smith Jr., W. O. (2007). Influence of sea ice cover and icebergs on circulation and water mass formation in a numerical circulation model of the ross sea, antarctica. *Journal of Geophysical Research: Oceans*, *112*(C11). Retrieved from `https://agupubs.onlinelibrary.wiley.com/doi/abs/10.1029/2006JC004036` doi: https://doi.org/10.1029/2006JC004036

Dinniman, M. S., St-Laurent, P., Arrigo, K. R., Hofmann, E. E., & van Dijken, G. L. (2020). Analysis of iron sources in antarctic continental shelf waters. *Journal of Geophysical Research: Oceans*, *125*(5), e2019JC015736. Retrieved from `https://agupubs.onlinelibrary.wiley.com/doi/abs/10.1029/2019JC015736` (e2019JC015736 2019JC015736) doi: https://doi.org/10.1029/2019JC015736

Durgadoo, J. V., Loveday, B. R., Reason, C. J. C., Penven, P., & Biastoch, A. (2013). Agulhas leakage predominantly responds to the southern hemisphere westerlies. *Journal of Physical Oceanography*, *43*(10), 2113 - 2131. Retrieved from `https://journals.ametsoc.org/view/journals/phoc/43/10/jpo-d-13-047.1.xml` doi: https://doi.org/10.1175/JPO-D-13-047.1

Feistel, R. (2012). Teos-10: A new international oceanographic standard for seawater, ice, fluid water, and humid air. *International Journal of Thermodynamics*, *33(8)*, 1335-1351. doi: 10.1007/s10765-010-0901-y

Foldvik, A., Gammelsrød, T., Østerhus, S., Fahrbach, E., Rohardt, G., Schröder, M., ... Woodgate, R. (2004). Ice shelf water overflow and bottom water formation in the southern weddell sea. *Journal of Geophysical Research: Oceans*, *109*(C2).

Fretwell, P., Pritchard, H. D., Vaughan, D. G., Bamber, J. L., Barrand, N. E., Bell, R., ... Zirizzotti, A. (2013). Bedmap2: improved ice bed, surface and thickness datasets for antarctica. *The Cryosphere*, *7*(1), 375–393. Retrieved from `https://tc.copernicus.org/articles/7/375/2013/` doi: 10.5194/tc-7-375-2013

Gade, H. G. (1979). *Melting of Ice in Sea Water: A Primitive Model with Application to the Antarctic Ice Shelf and Icebergs* (Vol. 9) (No. 1). doi: 10.1175/1520-0485(1979)009⟨0189:moiisw⟩2.0.co;2

Galton-Fenzi, B. K., Hunter, J. R., Coleman, R., Marsland, S. J., & Warner, R. C. (2012). Modeling the basal melting and marine ice accretion of the amery ice shelf. *Journal of Geophysical Research: Oceans*, *117*(C9). Retrieved from `https://agupubs.onlinelibrary.wiley.com/doi/abs/10.1029/2012JC008214` doi: https://doi.org/10.1029/2012JC008214

Gill, A. (1973). Circulation and bottom water production in the weddell sea. *Deep Sea Research and Oceanographic Abstracts*, *20*(2), 111-140. Retrieved from https://www.sciencedirect.com/science/article/pii/001174717390048X doi: https://doi.org/10.1016/0011-7471(73)90048-X

Good, S. A., Martin, M. J., & Rayner, N. A. (2013). En4: Quality controlled ocean temperature and salinity profiles and monthly objective analyses with uncertainty estimates. *Journal of Geophysical Research: Oceans*, *118*(12), 6704-6716. Retrieved from https://agupubs.onlinelibrary.wiley.com/doi/abs/10.1002/2013JC009067 doi: https://doi.org/10.1002/2013JC009067

Groeskamp, S., Zika, J. D., Sloyan, B. M., McDougall, T. J., & McIntosh, P. C. (2014). A thermohaline inverse method for estimating diathermohaline circulation and mixing. *Journal of Physical Oceanography*, *44*(10), 2681 - 2697. Retrieved from https://journals.ametsoc.org/view/journals/phoc/44/10/jpo-d-14-0039.1.xml doi: https://doi.org/10.1175/JPO-D-14-0039.1

Gunn, K. L., Rintoul, S. R., England, M. H., & Bowen, M. M. (2023). Recent reduced abyssal overturning and ventilation in the australian antarctic basin. *Nature*. Retrieved from https://www.nature.com/articles/s41558-023-01667-8 doi: https://doi.org/10.1038/s41558-023-01667-8

Guo, G., Shi, J., Gao, L., Tamura, T., & Williams, G. D. (2019). Reduced sea ice production due to upwelled oceanic heat flux in prydz bay, east antarctica. *Geophysical Research Letters*, *46(9)*(9), 4782-4789. Retrieved from https://agupubs.onlinelibrary.wiley.com/doi/abs/10.1029/2018GL081463 doi: 10.1029/2018GL081463

Hamming, R. W. (1973). Numerical methods for scientists and engineers. In (2nd ed., p. 721). New York: McGraw-Hill.

Herraiz-Borreguero, L., Church, J. A., Allison, I., Peña-Molino, B., Coleman, R., Tomczak, M., & Craven, M. (2016). Basal melt, seasonal water mass transformation, ocean current variability, and deep convection processes along the amery ice shelf calving front, east antarctica. *Journal of Geophysical Research: Oceans*, *121(7)*(7), 4946-4965. Retrieved from https://agupubs.onlinelibrary.wiley.com/doi/abs/10.1002/2016JC011858 doi: 10.1002/2016JC011858

Herraiz-Borreguero, L., Coleman, R., Allison, I., Rintoul, S. R., Craven, M., & Williams, G. D. (2015). Circulation of modified circumpolar deep water and basal melt beneath the amery ice shelf, east antarctica. *Journal of Geophysical Research: Oceans*, *120*(4), 3098-3112. Retrieved from https://agupubs.onlinelibrary.wiley.com/doi/abs/10.1002/2015JC010697 doi: 10.1002/2015JC010697

Heywood, K. J., Schmidtko, S., Heuzé, C., Kaiser, J., Jickells, T. D., Queste, B. Y., ... Smith, W. (2014). Ocean processes at the antarctic continental slope. *Philosophical Transactions of the Royal Society A: Mathematical, Physical and Engineering Sciences*, *372*(2019), 20130047. Retrieved from https://royalsocietypublishing.org/doi/abs/10.1098/rsta.2013.0047 doi: 10.1098/rsta.2013.0047

Holland, P. R. (2017). The transient response of ice shelf melting to ocean change. *Journal of Physical Oceanography*, *47*(8), 2101 - 2114. Retrieved from https://journals.ametsoc.org/view/journals/phoc/47/8/jpo-d-17-0071.1.xml doi: https://doi.org/10.1175/JPO-D-17-0071.1

Jackett, D. R., & McDougall, T. J. (1997). A neutral density variable for the world's oceans. *Journal of Physical Oceanography*, *27(2)*, 237 - 263. Retrieved from https://journals.ametsoc.org/view/journals/phoc/27/2/1520-0485_1997_027_0237_andvft_2.0.co_2.xml doi: 10.1175/1520-0485

Jacobs, S. S. (2004). Bottom water production and its links with the thermohaline circulation. *Antarctic Science*, *16(4)*(4), 427-437. doi: 10.1017/S095410200400224X

Jacobs, S. S., Helmer, H. H., Doake, C. S., Jenkins, A., & Frolich, R. M. (1992). Melting of ice shelves and the mass balance of Antarctica. *Journal of Glaciology*, *38*(130), 375–387. doi: 10.1017/S0022143000002252

Jia, R., Chen, M., Pan, H., Zeng, J., Zhu, J., Liu, X., ... Qiu, Y. (2022). Freshwater components track the export of dense shelf water from prydz bay, antarctica. *Deep Sea Research Part II: Topical Studies in Oceanography*, *196*, 105023. Retrieved from https://www.sciencedirect.com/science/article/pii/S096706452200008X doi: 10.1016/j.dsr2.2022.105023

Klinck, J. M., & Dinniman, M. S. (2010). Exchange across the shelf break at high southern latitudes. *Ocean Science*, *6*(2), 513–524. Retrieved from https://os.copernicus.org/articles/6/513/2010/ doi: 10.5194/os-6-513-2010

Kusahara, K., Hasumi, H., & Tamura, T. (2010). Modeling sea ice production and dense shelf water formation in coastal polynyas around east antarctica. *Journal of Geophysical Research: Oceans*, *115*(C10). Retrieved from https://agupubs.onlinelibrary.wiley.com/doi/abs/10.1029/2010JC006133 doi: https://doi.org/10.1029/2010JC006133

Kusahara, K., Williams, G. D., Tamura, T., Massom, R., & Hasumi, H. (2017). Dense shelf water spreading from antarctic coastal polynyas to the deep southern ocean: A regional circumpolar model study. *Journal of Geophysical Research: Oceans*, *122*(8), 6238-6253. Retrieved from https://agupubs.onlinelibrary.wiley.com/doi/abs/10.1002/2017JC012911 doi: https://doi.org/10.1002/2017JC012911

Lacarra, M., Houssais, M.-N., Herbaut, C., Sultan, E., & Beauverger, M. (2014). Dense shelf water production in the adélie depression, east antarctica, 2004–2012: Impact of the mertz glacier calving. *Journal of Geophysical Research: Oceans*, *119*(8), 5203-5220. Retrieved from https://agupubs.onlinelibrary.wiley.com/doi/abs/10.1002/2013JC009124 doi: https://doi.org/10.1002/2013JC009124

Li, Q., England, M. H., Hogg, A. M., Rintoul, S. R., & Morrison, A. K. (2023). Abyssal ocean overturning slowdown and warming driven by antarctic meltwater. *Nature*, *615*, 841–847. Retrieved from https://www.nature.com/articles/s41586-023-05762-w#citeas doi: 10.1038/s41586-023-05762-w

Liu, C., Wang, Z., Cheng, C., Xia, R., Li, B., & Xie, Z. (2017). Modeling modified circumpolar deep water intrusions onto the prydz bay continental shelf, east antarctica. *Journal of Geophysical Research: Oceans*, *122*(7), 5198-5217. Retrieved from https://agupubs.onlinelibrary.wiley.com/doi/abs/10.1002/2016JC012336 doi: https://doi.org/10.1002/2016JC012336

Malik, N. A., Dracos, T., & Papantoniou, D. A. (1993). Particle tracking velocimetry in three-dimensional flows. part ii: Particle tracking. *Experiments in Fluids*, *15*, 279–294. Retrieved from https://link.springer.com/article/10.1007/BF00223406#citeas doi: 10.1007/BF00223406

Martin, S. (2019). Polynyas. In J. K. Cochran, H. J. Bokuniewicz, & P. L. Yager (Eds.), *Encyclopedia of ocean sciences (third edition)* (Third Edition ed., p. 175-180). Oxford: Academic Press. Retrieved from https://www.sciencedirect.com/science/article/pii/B9780124095489114770 doi: 10.1016/B978-0-12-409548-9.11477-0

McDougall, T. J., & Barker, P. (2011). Getting started with teos-10 and the gibbs seawater (gsw) oceanographic toolbox. *SCOR/IAPSO WG*, *127*, 1-28.

McDougall, T. J., Barker, P. M., Feistel, R., & Galton-Fenzi, B. K. (2014). Melting of ice and sea ice into seawater and frazil ice formation. *Journal of Physical Oceanography*, *44*(7), 1751 - 1775. Retrieved from https://journals.ametsoc.org/view/journals/phoc/44/7/jpo-d-13-0253.1.xml doi: https://doi.org/10.1175/JPO-D-13-0253.1

Menemenlis, D., Campin, J., Heimbach, P., Hill, C., Lee, T., Nguyen, A., ... Zhang, H. (2008). ECCO2: High Resolution Global Ocean and Sea Ice Data Synthesis. In *Agu fall meeting abstracts* (pp. OS31C–1292). Retrieved from https://ui.adsabs.harvard.edu/abs/2008AGUFMOS31C1292M

Morrison, A. K., Hogg, A. M., England, M. H., & Spence, P. (2020). Warm circumpolar deep water transport toward antarctica driven by local dense water export in canyons. *Science Advances*, *6*(18), eaav2516. Retrieved from https://www.science.org/doi/abs/10.1126/sciadv.aav2516 doi: 10.1126/sciadv.aav2516

Narayanan, A., Gille, S. T., Mazloff, M. R., & Murali, K. (2019). Water mass characteristics of the antarctic margins and the production and seasonality of dense shelf water. *Journal of Geophysical Research: Oceans*, *124*(12), 9277-9294. Retrieved from https://agupubs.onlinelibrary.wiley.com/doi/abs/10.1029/2018JC014907 doi: 10.1029/2018JC014907

Nunes Vaz, R. A., & Lennon, G. W. (1996). Physical oceanography of the prydz bay region of antarctic waters. *Deep Sea Research Part I: Oceanographic Research Papers*, *43(5)*. Retrieved from http://www.ccpo.odu.edu/~klinck/Reprints/PDF/nunesvazDSR1996.pdf doi: 10.1016/0967-0637(96)00028-3

Ohshima, K. I., Fukamachi, Y., Williams, G. D., Nihashi, S., Roquet, F., Kitade, Y., ... Wakatsuchi, M. (2013). Antarctic bottom water production by intense sea-ice formation in the cape darnley polynya. *Nature Geoscience*, *6*, 235–240. doi: https://doi.org/10.1038/ngeo1738

Ohshima, K. I., Nihashi, S., & Iwamoto, K. (2016). Global view of sea-ice production in polynyas and its linkage to dense/bottom water formation. *Geoscience Letters*, *3*. doi: 10.1186/s40562-016-0045-4

Orsi, A. H., Johnson, G. C., & Bullister, J. L. (1999, January). Circulation, mixing, and production of antarctic bottom water. *Progress in Oceanography*, *43(1)*(1), 55-109. doi: 10.1016/S0079-6611(99)00004-X

Orsi, A. H., & Whitworth, T. I. (2005). Hydrographic atlas of the world ocean circulation experiment (woce) volume 1: Southern ocean. In (Vol. 1, p. 223). WOCE International Project Office.

Pedregosa, F., Varoquaux, G., Gramfort, A., Michel, V., Thirion, B., Grisel, O., ... Duchesnay, E. (2011). Scikit-learn: Machine learning in Python. *Journal of Machine Learning Research*, *12*, 2825–2830.

Pellichero, V., Sallée, J.-B., Chapman, C. C., & Downes, S. M. (2018). The southern ocean meridional overturning in the sea-ice sector is driven by freshwater fluxes. *Nature Communications*, *9(1):1789*. doi: 10.1038/s41467-018-04101-2

Peña-Molino, B., McCartney, M. S., & Rintoul, S. R. (2016). Direct observations of the antarctic slope current transport at 113°e. *Journal of Geophysical Research: Oceans*, *121*(10), 7390-7407. Retrieved from https://agupubs.onlinelibrary.wiley.com/doi/abs/10.1002/2015JC011594 doi: https://doi.org/10.1002/2015JC011594

Piñones, A., Hofmann, E. E., Dinniman, M. S., & Klinck, J. M. (2011). Lagrangian simulation of transport pathways and residence times along the western antarctic peninsula. *Deep Sea Research Part II: Topical Studies in Oceanography*, *58(13-16)*, 1524-1539. Retrieved from https://www.sciencedirect.com/science/article/pii/S0967064510003796 (Understanding the Linkages between Antarctic Food Webs and the Environment: A Synthesis of Southern Ocean GLOBEC Studies) doi: 10.1016/j.dsr2.2010.07.001

Portela, E., Rintoul, S. R., Bestley, S., Herraiz-Borreguero, L., van Wijk, E., McMahon, C. R., ... Hindell, M. (2021). Seasonal transformation and spatial variability of water masses within mackenzie polynya, prydz bay. *Journal of Geophysical Research: Oceans*, *126*(12), e2021JC017748. Retrieved from https://agupubs.onlinelibrary.wiley.com/doi/abs/10.1029/2021JC017748 (e2021JC017748 2021JC017748) doi: https://doi.org/10.1029/2021JC017748

Portela, E., Rintoul, S. R., Herraiz-Borreguero, L., Roquet, F., Bestley, S., van Wijk, E., ... Hindell, M. A. (2022). Controls on dense shelf water formation in four east antarctic polynyas. *Journal of Geophysical Research: Oceans*, *127*(12), e2022JC018804. Retrieved from https://agupubs.onlinelibrary.wiley.com/doi/abs/10.1029/2022JC018804 (e2022JC018804 2022JC018804) doi: 10.1029/2022JC018804

Purkey, S. G., & Johnson, G. C. (2013). Antarctic bottom water warming and freshening: Contributions to sea level rise, ocean freshwater budgets, and global heat gain. *Journal of Climate*, *26*(16), 6105–6122. doi: 10.1175/JCLI-D-12-00834.1

Ribeiro, N., Herraiz-Borreguero, L., Rintoul, S. R., McMahon, C. R., Hindell, M., Harcourt, R., & Williams, G. (2021). Warm modified circumpolar deep water intrusions drive ice shelf melt and inhibit dense shelf water formation in vincennes bay, east antarctica. *Journal of Geophysical Research: Oceans*, *126*(8), e2020JC016998. Retrieved from https://agupubs.onlinelibrary.wiley.com/doi/abs/10.1029/2020JC016998 (e2020JC016998 2020JC016998) doi: https://doi.org/10.1029/2020JC016998

Richter, O., Gwyther, D. E., Galton-Fenzi, B. K., & Naughten, K. A. (2022). The whole antarctic ocean model (waom v1.0): development and evaluation. *Geoscientific Model Development*, *15*(2), 617–647. Retrieved from https://gmd.copernicus.org/articles/15/617/2022/ doi: 10.5194/gmd-15-617-2022

Roquet, F., Madec, G., McDougall, T. J., & Barker, P. (2015). Accurate polynomial expressions for the density and specific volume of seawater using the teos-10 standard. *Ocean Modelling*. doi: 10.1016/j.ocemod.2015.04.002

Rühs, S., Durgadoo, J. V., Behrens, E., & Biastoch, A. (2013). Advective timescales and pathways of agulhas leakage. *Geophysical Research Letters*, *40(15)*(15), 3997-4000. doi: 10.1002/grl.50782

Sallée, J.-B., Speer, K., Rintoul, S., & Wijffels, S. (2010). Southern ocean thermocline ventilation. *Journal of Physical Oceanography*, *40(3)*, 509 - 529. Retrieved from https://journals.ametsoc.org/view/journals/phoc/40/3/2009jpo4291.1.xml doi: 10.1175/2009JPO4291.1

Schaffer, J., Timmermann, R., Arndt, J. E., Kristensen, S. S., Mayer, C., Morlighem, M., & Steinhage, D. (2016). A global, high-resolution data set of ice sheet topography, cavity geometry, and ocean bathymetry. *Earth System Science Data*, *8*(2), 543–557. Retrieved from https://essd.copernicus.org/articles/8/543/2016/ doi: 10.5194/essd-8-543-2016

Schmidtko, S., Heywood, K. J., Thompson, A. F., & Aoki, S. (2014). Multidecadal warming of antarctic waters. *Science*, *346*(6214), 1227-1231. Retrieved from https://www.science.org/doi/abs/10.1126/science.1256117 doi: 10.1126/science.1256117

Schroeter, S., O'Kane, T. J., & Sandery, P. A. (2022, 9). Antarctic sea ice regime shift associated with decreasing zonal symmetry in the southern annular mode. *The Cryosphere*. doi: https://doi.org/10.5194/tc-2022-151

Shanmugam, G. (2021). Chapter 8 - bottom currents. In G. Shanmugam (Ed.), *Mass transport, gravity flows, and bottom currents* (p. 309-375). Elsevier. Retrieved from https://www.sciencedirect.com/science/article/pii/B9780128225769000084 doi: https://doi.org/10.1016/B978-0-12-822576-9.00008-4

Shchepetkin, A. F., & McWilliams, J. C. (2009). Correction and commentary for "ocean forecasting in terrain-following coordinates: Formulation and skill assessment of the regional ocean modeling system" by haidvogel et al., j. comp. phys. 227, pp. 3595–3624. *Journal of Computational Physics*, *228*(24), 8985-9000. Retrieved from https://www.sciencedirect.com/science/article/pii/S0021999109004872 doi: https://doi.org/10.1016/j.jcp.2009.09.002

Silvano, A., Rintoul, S. R., Peña-Molino, B., Hobbs, W. R., van Wijk, E., Aoki, S., . . . Williams, G. D. (2018). Freshening by glacial meltwater enhances melting of ice shelves and reduces formation of antarctic bottom water. *Science advances*, *4(4)*. doi: 10.1126/sciadv.aap9467

Solodoch, A., Stewart, A. L., Hogg, A. M., Morrison, A. K., Kiss, A. E., Thompson, A. F., ... Cimoli, L. (2022). How does antarctic bottom water cross the southern ocean? *Geophysical Research Letters*, *49*(7), e2021GL097211. Retrieved from https://agupubs.onlinelibrary.wiley.com/doi/abs/10.1029/2021GL097211 (e2021GL097211 2021GL097211) doi: 10.1029/2021GL097211

Stanley, G. J. (2019). Neutral surface topology. *Ocean Modelling*, *138*, 88-106. Retrieved from https://www.sciencedirect.com/science/article/pii/S1463500318302221 doi: https://doi.org/10.1016/j.ocemod.2019.01.008

Talley, L. D., Pickard, G. L., Emery, W. J., & Swift, J. H. (2011). Chapter 13 - southern ocean. In L. D. Talley, G. L. Pickard, W. J. Emery, & J. H. Swift (Eds.), *Descriptive physical oceanography (sixth edition)* (Sixth Edition ed., p. 437-471). Boston: Academic Press. Retrieved from https://www.sciencedirect.com/science/article/pii/B9780750645522100137 doi: https://doi.org/10.1016/B978-0-7506-4552-2.10013-7

Tamsitt, V., Abernathey, R. P., Mazloff, M. R., Wang, J., & Talley, L. D. (2018). Transformation of deep water masses along lagrangian upwelling pathways in the southern ocean. *Journal of Geophysical Research: Oceans*, *123(3)*(3), 1994-2017. Retrieved from https://agupubs.onlinelibrary.wiley.com/doi/abs/10.1002/2017JC013409 doi: 10.1002/2017JC013409

Tamsitt, V., England, M. H., Rintoul, S. R., & Morrison, A. K. (2021). Residence time and transformation of warm circumpolar deep water on the antarctic continental shelf. *Geophysical Research Letters*, *48*(20), e2021GL096092. Retrieved from https://agupubs.onlinelibrary.wiley.com/doi/abs/10.1029/2021GL096092 (e2021GL096092 2021GL096092) doi: https://doi.org/10.1029/2021GL096092

Tamura, T., Ohshima, K. I., Fraser, A. D., & Williams, G. D. (2016). Sea ice production variability in antarctic coastal polynyas. *Journal of Geophysical Research: Oceans*, *121(5)*(5), 2967-2979. Retrieved from https://agupubs.onlinelibrary.wiley.com/doi/abs/10.1002/2015JC011537 doi: 10.1002/2015JC011537

Tamura, T., Ohshima, K. I., & Nihashi, S. (2008). Mapping of sea ice production for antarctic coastal polynyas. *Geophysical Research Letters*, *35*(7). Retrieved from https://agupubs.onlinelibrary.wiley.com/doi/abs/10.1029/2007GL032903 doi: 10.1029/2007GL032903

Tamura, T., Ohshima, K. I., Nihashi, S., & Hasumi, H. (2011). Estimation of surface heat/salt fluxes associated with sea ice growth/melt in the southern ocean. *SOLA*, *7*, 17-20. doi: 10.2151/sola.2011-005

Thompson, A. F., Stewart, A. L., Spence, P., & Heywood, K. J. (2018). The antarctic slope current in a changing climate. *Reviews of Geophysics*, *56*(4), 741-770. Retrieved from https://agupubs.onlinelibrary.wiley.com/doi/abs/10.1029/2018RG000624 doi: 10.1029/2018RG000624

van Sebille, E., Griffies, S. M., Abernathey, R., Adams, T. P., Berloff, P., Biastoc, A., ... Zika, J. D. (2018, January). Lagrangian ocean analysis: Fundamentals and practices. *Ocean Modeling*(121), 49–75. doi: 10.1016/j.ocemod.2017.11.008

van Sebille, E., Spence, P., Mazloff, M. R., England, M. H., Rintoul, S. R., & Saenko, O. A. (2013). Abyssal connections of antarctic bottom water in a southern ocean state estimate. *Geophysical Research Letters*, *40(10)*(10), 2177-2182. Retrieved from https://agupubs.onlinelibrary.wiley.com/doi/abs/10.1002/grl.50483 doi: 10.1002/grl.50483

van Wijk, E. M., & Rintoul, S. R. (2014). Freshening drives contraction of antarctic bottom water in the australian antarctic basin. *Geophysical Research Letters*, *41*(5), 1657-1664. Retrieved from https://agupubs

.onlinelibrary.wiley.com/doi/abs/10.1002/2013GL058921 doi: https://doi.org/10.1002/2013GL058921

Viglione, G. A., & Thompson, A. F. (2016). Lagrangian pathways of upwelling in the southern ocean. *Journal of Geophysical Research: Oceans*, *121*(8), 6295-6309. Retrieved from https://agupubs.onlinelibrary.wiley.com/doi/abs/10.1002/2016JC011773 doi: 10.1002/2016JC011773

Ward, J. H. J. (1963). Hierarchical grouping to optimize an objective function. *Journal of the American Statistical Association*, *58*(301), 236-244. doi: 10.1080/01621459.1963.10500845

Williams, G. D., Herraiz-Borreguero, L., Roquet, F., Tamura, T., Ohshima, K. I., Fukamachi, Y., ... Hindell, M. (2016). The suppression of antarctic bottom water formation by melting ice shelves in prydz bay. *Nature Communications*, *7(12577)*. Retrieved from https://www.ncbi.nlm.nih.gov/pmc/articles/PMC4996980/ doi: 10.1038/ncomms12577

Yoon, S.-T., Lee, W. S., Stevens, C., Jendersie, S., Nam, S., Yun, S., ... Lee, J. (2020). Variability in high-salinity shelf water production in the terra nova bay polynya, antarctica. *Ocean Science*, *16*(2), 373–388. Retrieved from https://os.copernicus.org/articles/16/373/2020/ doi: 10.5194/os-16-373-2020

Zhou, S., Meijers, A. J. S., Meredith, M. P., Abrahamsen, E. P., Holland, P. R., Silvano, A., ... Østerhus, S. (2023). Slowdown of antarctic bottom water export driven by climatic wind and sea-ice changes. *Nature*, *13*, 701–709. Retrieved from https://www.nature.com/articles/s41558-023-01695-4#citeas doi: https://doi.org/10.1038/s41558-023-01695-4

Figure 4.

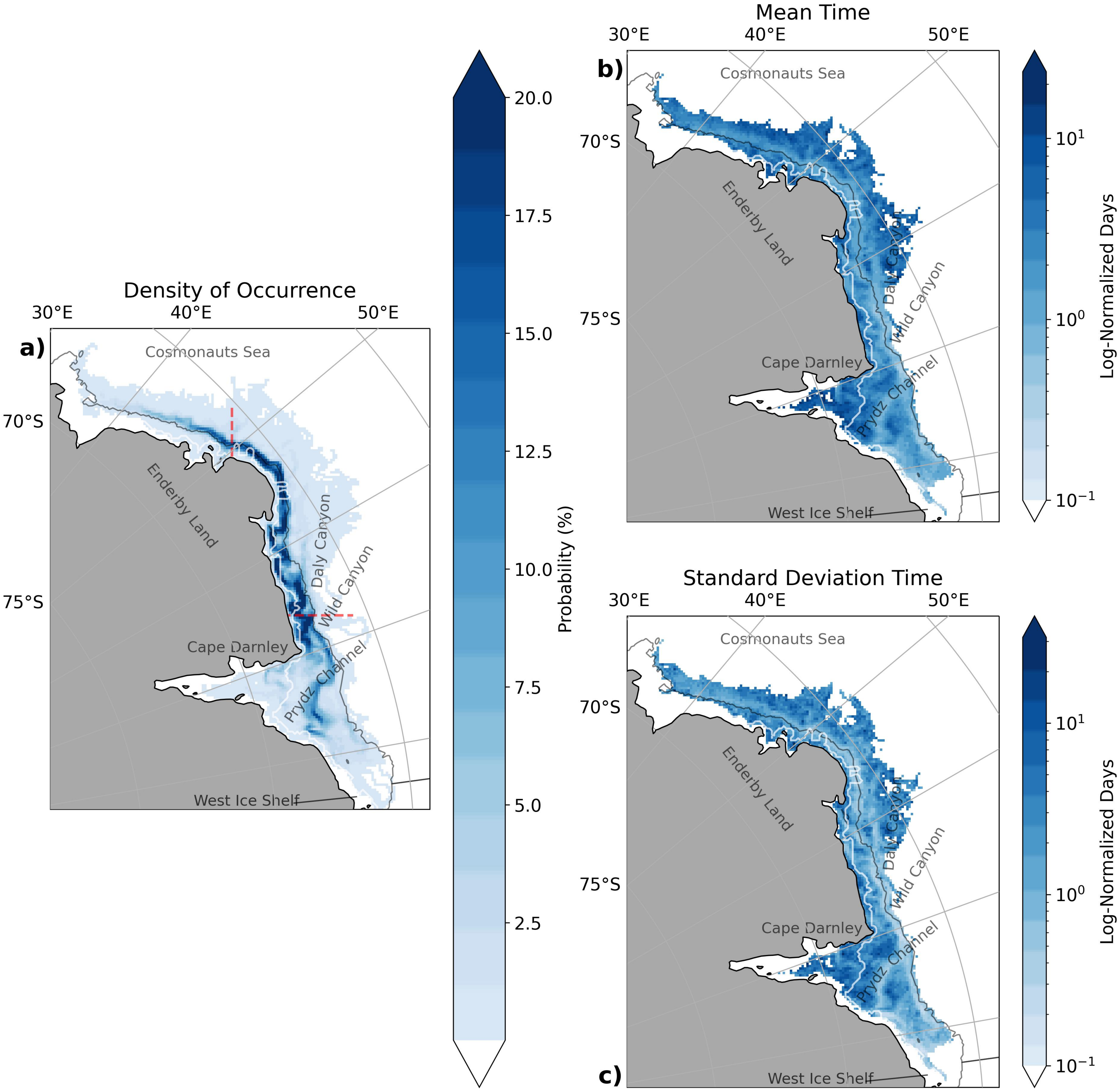

Density of Occurrence
a)
30°E
40°E
50°E
70°S
75°S
Cosmonauts Sea
Enderby Land
Daly Canyon
Wild Canyon
Cape Darnley
Prydz Channel
West Ice Shelf
Probability (%)
20.0
17.5
15.0
12.5
10.0
7.5
5.0
2.5
Mean Time
b)
Standard Deviation Time
c)
Log-Normalized Days
10^1
10^0
10^{-1}

Figure 1.

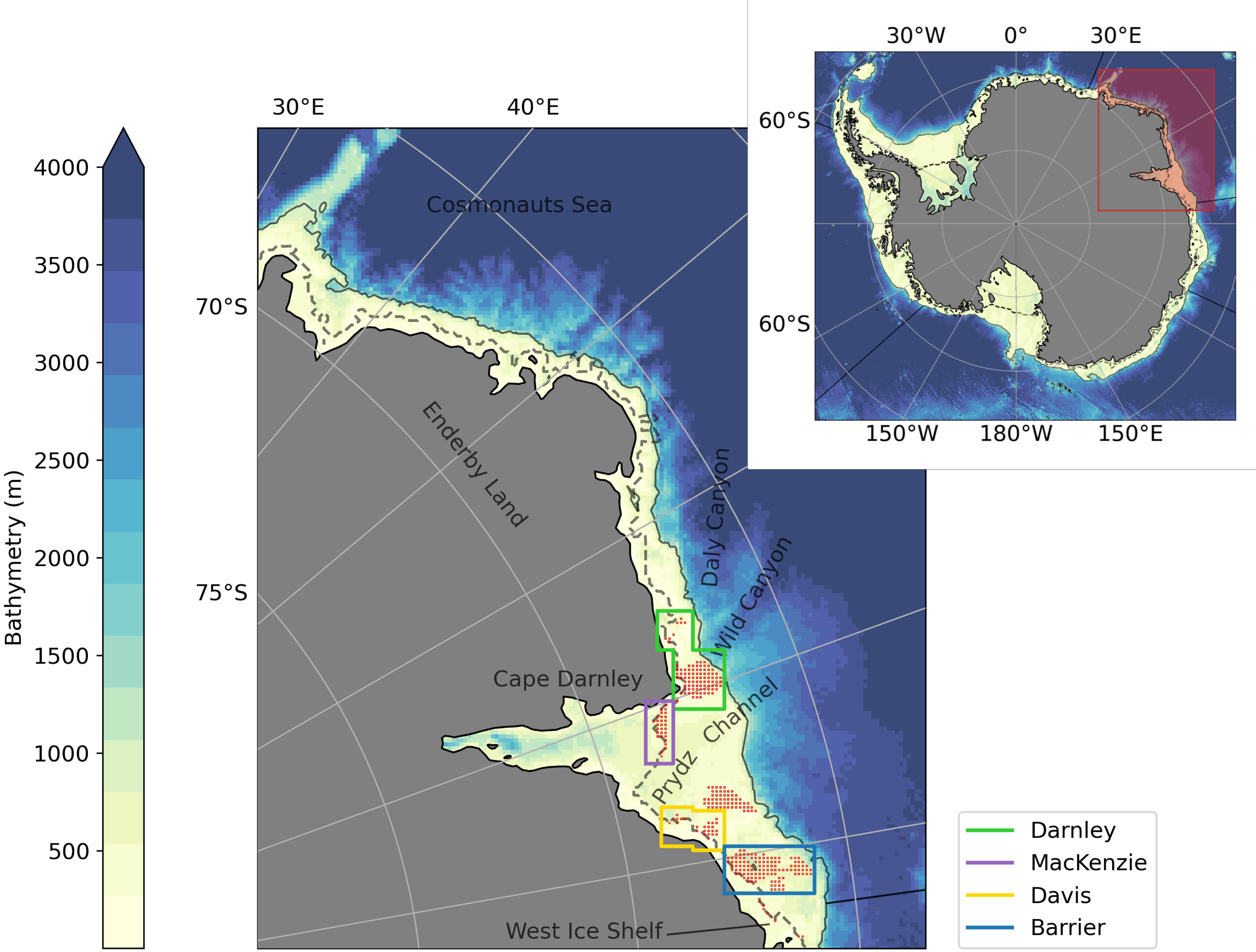

Bathymetry (m)
4000
3500
3000
2500
2000
1500
1000
500
30°E
40°E
70°S
75°S
Cosmonauts Sea
Enderby Land
Daly Canyon
Wild Canyon
Cape Darnley
Prydz Channel
West Ice Shelf
30°W
0°
30°E
60°S
60°S
150°W
180°W
150°E
Darnley
MacKenzie
Davis
Barrier

Figure 5.

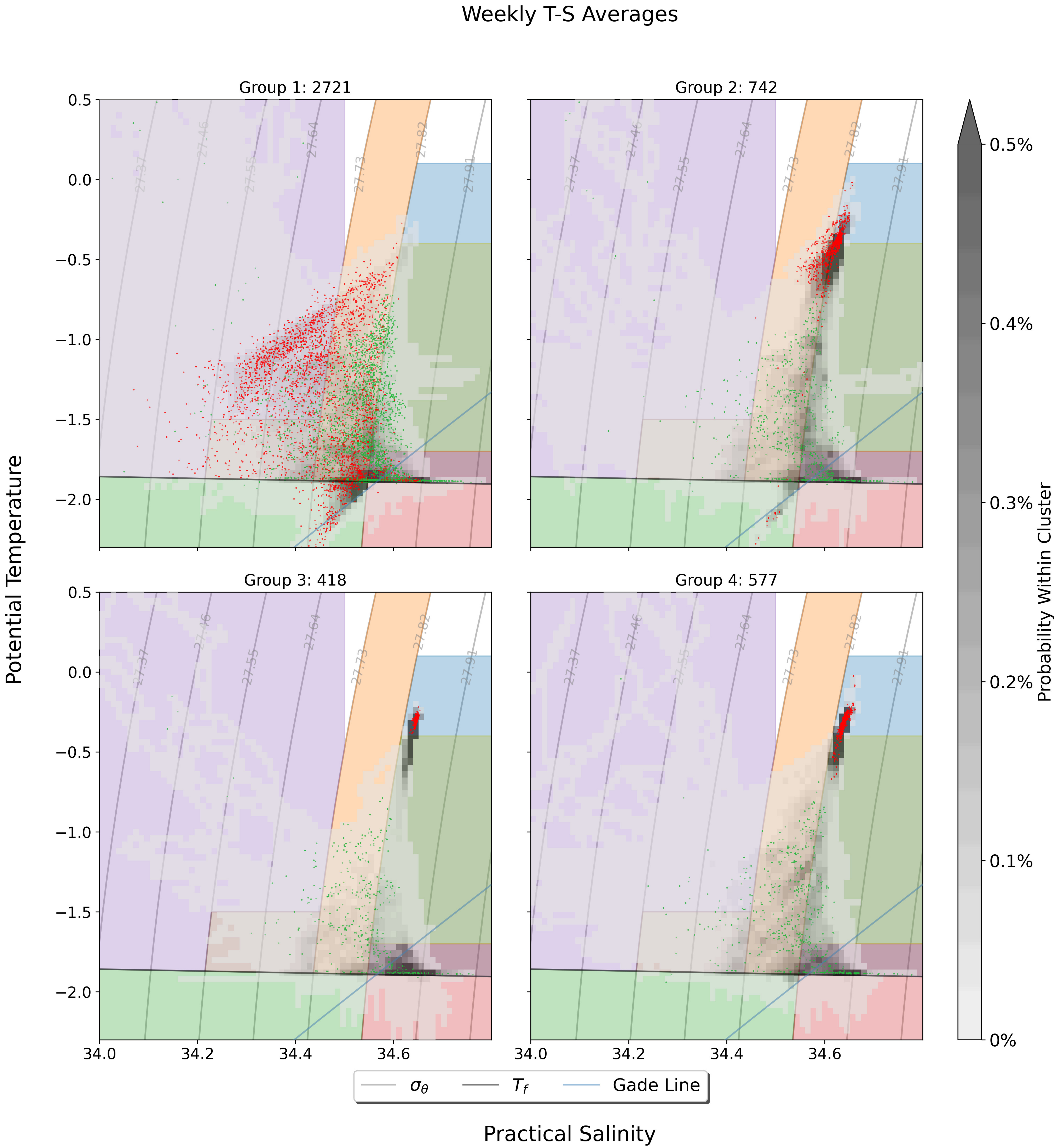

Weekly T-S Averages
Group 1: 2721
Group 2: 742
Group 3: 418
Group 4: 577
27.37
27.46
27.55
27.64
27.73
27.82
27.91
Potential Temperature
Practical Salinity
Probability Within Cluster
0.5%
0.4%
0.3%
0.2%
0.1%
0%
σ_θ
T_f
Gade Line

Figure 3.

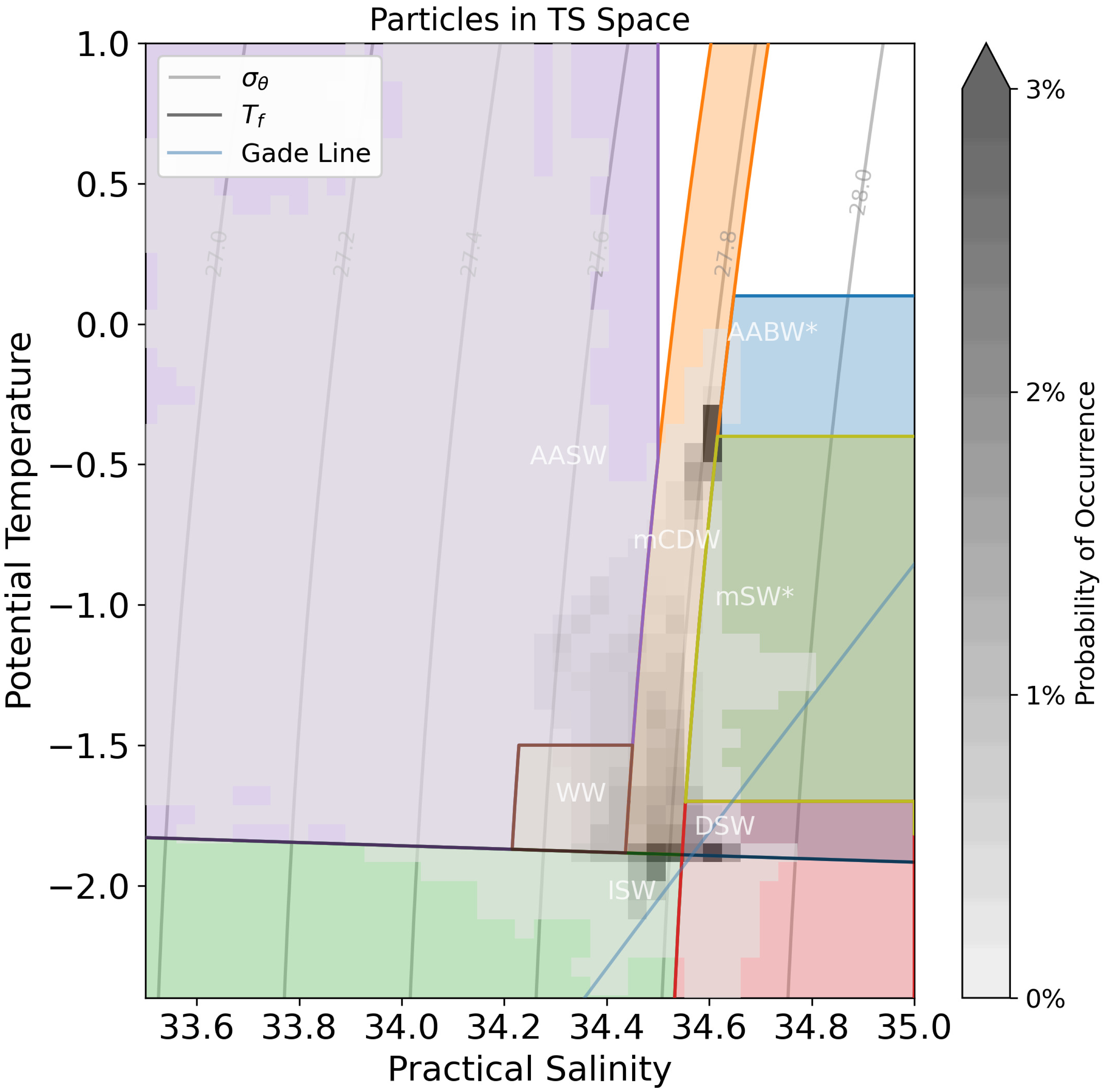

Particles in TS Space
σ_θ
T_f
Gade Line
27.0
27.2
27.4
27.6
27.8
28.0
AASW
AABW*
mCDW
mSW*
WW
DSW
ISW
Potential Temperature
Practical Salinity
Probability of Occurrence
3%
2%
1%
0%
1.0
0.5
0.0
−0.5
−1.0
−1.5
−2.0
33.6
33.8
34.0
34.2
34.4
34.6
34.8
35.0

Figure 7.

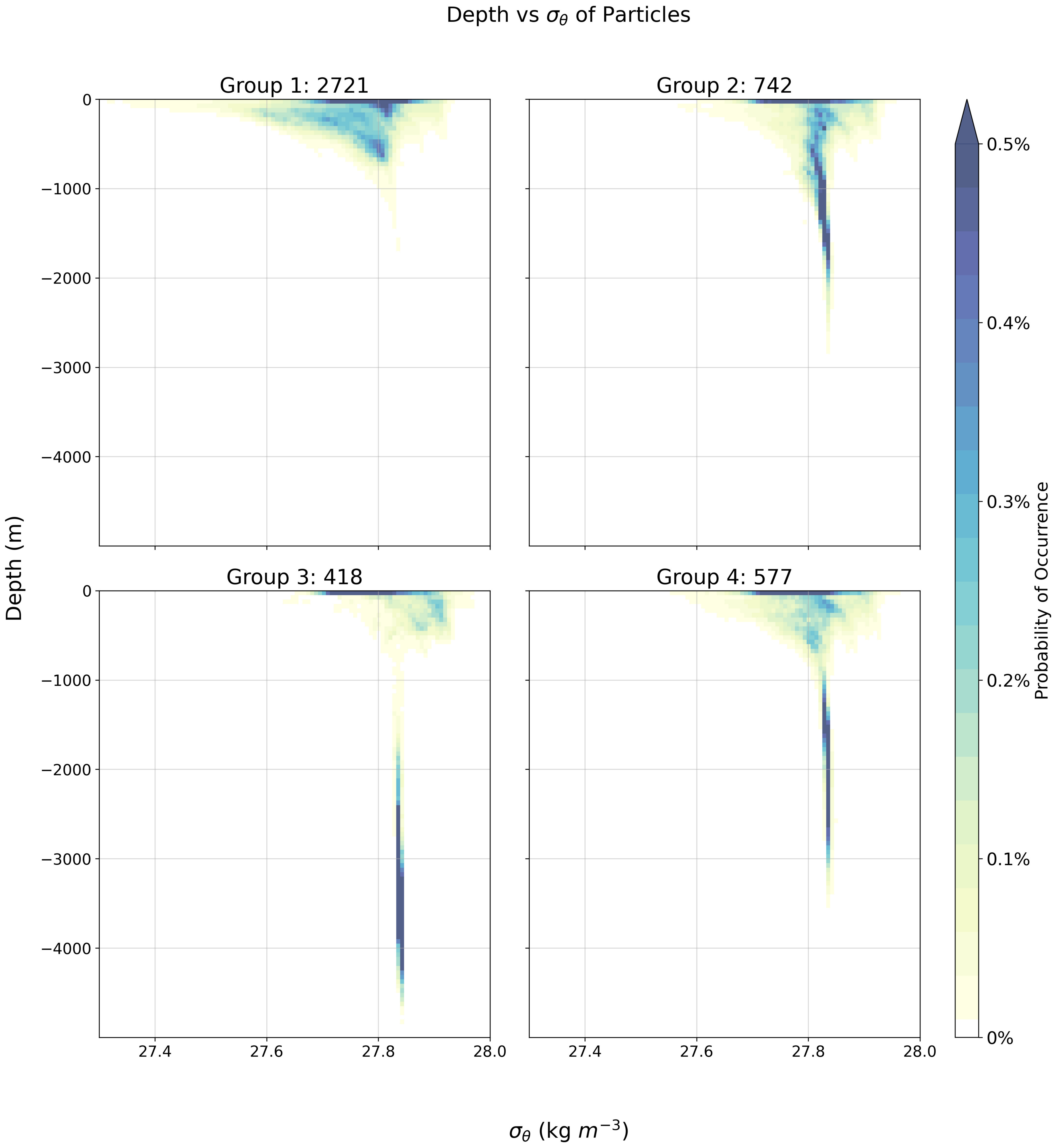

Depth vs σ_θ of Particles
Group 1: 2721
Group 2: 742
Group 3: 418
Group 4: 577
Depth (m)
0
−1000
−2000
−3000
−4000
27.4
27.6
27.8
28.0
σ_θ (kg m^{-3})
Probability of Occurrence
0%
0.1%
0.2%
0.3%
0.4%
0.5%

Figure 2.

Particle Release Date Distribution
% of Polynya-released Particles
25%
15%
5%
Darnley
MacKenzie
Davis
Barrier
Unnamed, East
Number of Particles
350
300
250
200
150
100
50
0
4
12
20
28
36
44
52
Week of the Year

Figure 6.

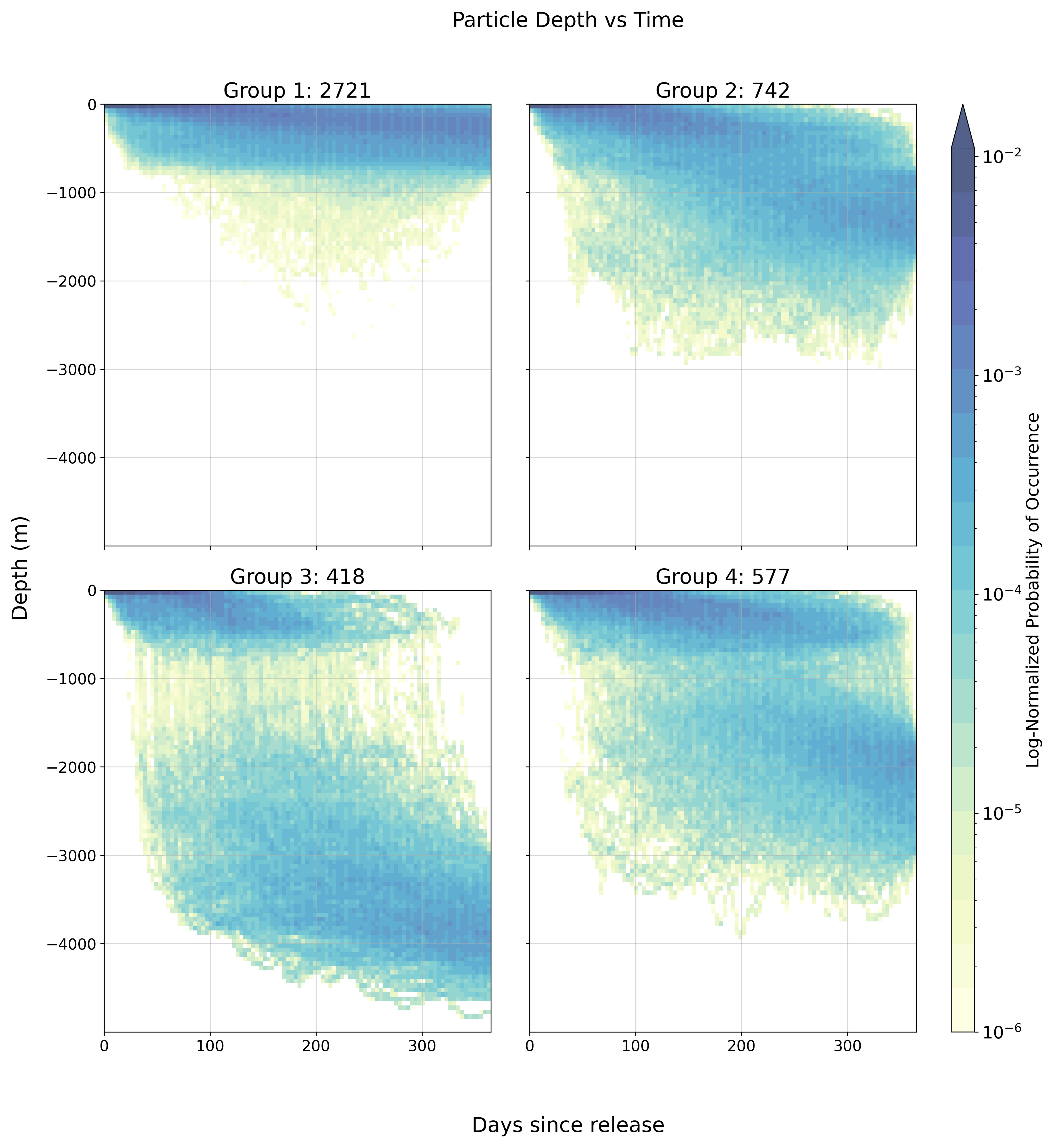
Particle Depth vs Time
Group 1: 2721
Group 2: 742
Group 3: 418
Group 4: 577
Depth (m)
0
−1000
−2000
−3000
−4000
0
100
200
300
Days since release
Log-Normalized Probability of Occurrence
10^{-2}
10^{-3}
10^{-4}
10^{-5}
10^{-6}

Figure 8.

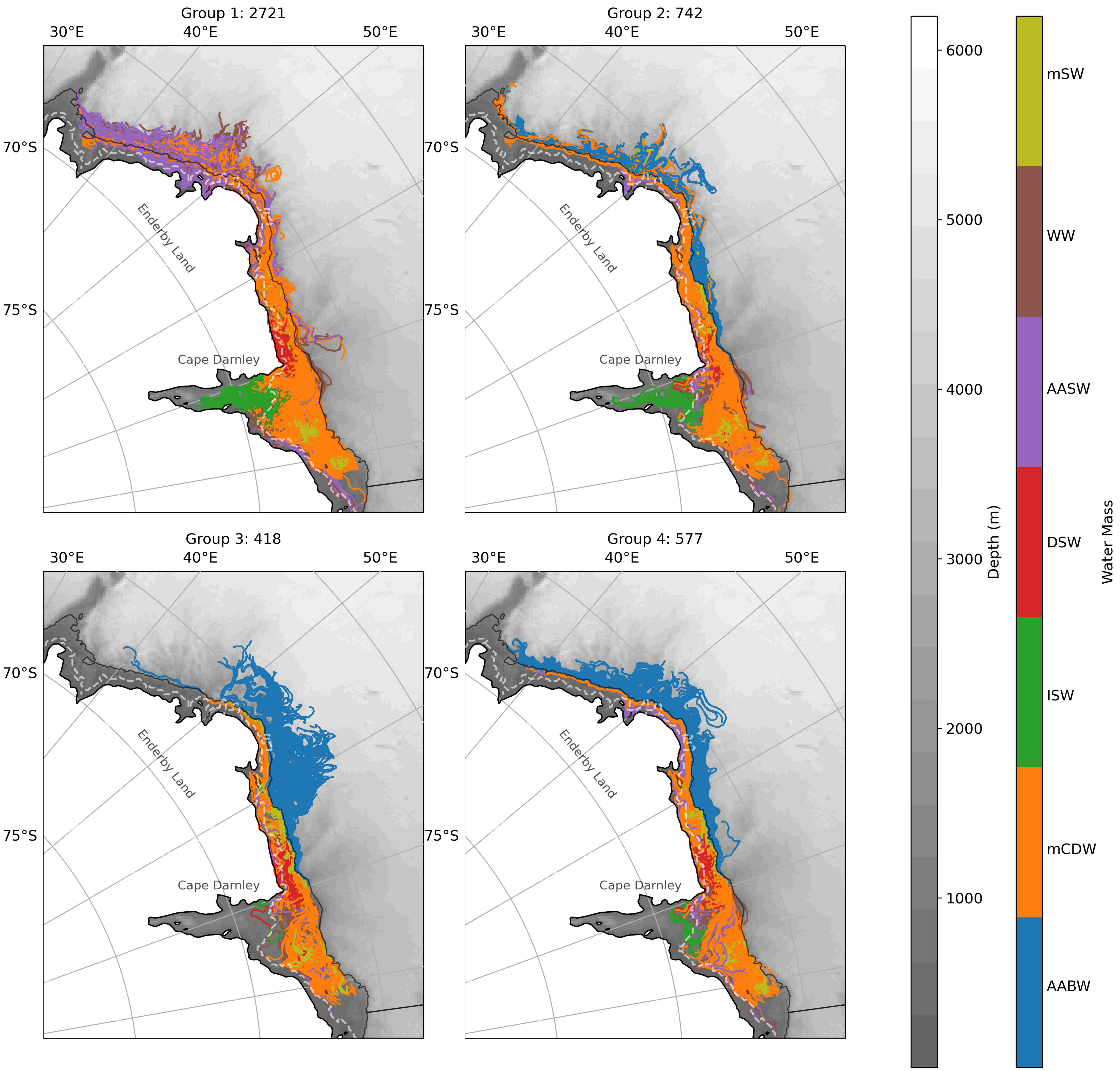

Group 1: 2721
Group 2: 742
Group 3: 418
Group 4: 577
30°E
40°E
50°E
70°S
75°S
Enderby Land
Cape Darnley
Depth (m)
6000
5000
4000
3000
2000
1000
Water Mass
mSW
WW
AASW
DSW
ISW
mCDW
AABW

Figure 9.


68 ° E - Annual Mean
50 ° E - Annual Mean
Depth (m)
Latitude
θ
S
σθ
0
−200
−400
−600
−800
−1000
−1200
−1400
−67.5
−67.0
−66.5
−66.0
−66.4
−66.2
−66.0
−65.8
−65.6
−65.4
0.6
0.1
−0.4
−0.9
−1.4
−1.9
34.7
34.6
34.5
34.4
34.3
34.2
34.1
34.0
33.9
33.8
27.71
27.65
27.59
27.53
27.47
27.41
27.35
27.29
27.23
27.17